

Article

Antimicrobial Properties of Zinc Oxide Nanoparticles Synthesized from *Lavandula pubescens* Shoot Methanol Extract

Abu ElGasim A. Yagoub ¹, Ghedeir M. Al-Shammari ^{1,*}, Laila Naif Al-Harbi ¹, Pandurangan Subash-Babu ¹, Rasha Elsayim ², Mohammed A. Mohammed ¹, Mohammed Abdo Yahya ¹ and Sndos Z. A. Fattiny ¹

¹ Department of Food Science and Nutrition, College of Food and Agriculture Sciences, King Saud University, P.O. Box 2460, Riyadh 11451, Saudi Arabia

² Department of Microbiology, College of Sciences, King Saud University, P.O. Box 2460, Riyadh 11451, Saudi Arabia

* Correspondence: aghedeir@ksu.edu.sa

Abstract: We report on employing in vitro biosynthesized ZnO nanoparticles using *L. pubescens* shoot methanol extract (50 and 100 mg LP–ZnO NPs) to examine their antimicrobial efficacy against *Pseudomonas aeruginosa* (ATCC27853), *Staphylococcus aureus* (ATCC 29213), *Aspergillus niger* (ATCC 16404 NA), and *Aspergillus terreus* (TCC 10029). The formation and stability of the investigated ZnO nanoparticles were proven by transmission electron microscopy (TEM), Fourier-transform infrared spectroscopy (FT-IR), UV–vis spectroscopy, X-ray diffraction (XRD), and thermal gravimetric analysis (TGA). The ZnO nanoparticles were rod-shaped (width: 10.76–30.93 nm). The nanoparticles in dimethyl sulfoxide (DMSO) outperformed their water counterparts in terms of their zones of inhibition (ZIs) (marginal means of 12.5 and 8.19 mm, respectively) and minimum inhibition concentrations (MICs) (means of 4.40 and 8.54 mg/mL, respectively). The ZI means for *S. aureus*, *P. aeruginosa*, *A. terreus*, and *A. niger* were 10.50, 6.13, 12.5, and 11.5 mm, respectively. When treating *S. aureus* and *P. aeruginosa*, the ZI of the 50 mg LP–ZnO NPs in water was better (14 mm), with a lower MIC and lower minimum bactericidal/fungicide concentrations (MBC/MFC) (7.22 and 4.88 mg/mL, respectively) than the ZnO and control drugs. The SEM images showed cellular alterations in the surface shapes after the LP–ZnO-NP treatments. Biosynthesized LP–ZnO NPs could have beneficial antibacterial properties, which could allow for future contributions to the development of new antimicrobial drugs.

Keywords: lavender shoots; bioactive compounds; biosynthesis; ZnO nanorod; zone of inhibition



Citation: Yagoub, A.E.A.; Al-Shammari, G.M.; Al-Harbi, L.N.; Subash-Babu, P.; Elsayim, R.; Mohammed, M.A.; Yahya, M.A.; Fattiny, S.Z.A. Antimicrobial Properties of Zinc Oxide Nanoparticles Synthesized from *Lavandula pubescens* Shoot Methanol Extract. *Appl. Sci.* **2022**, *12*, 11613. <https://doi.org/10.3390/app122211613>

Academic Editor: Leonarda Liotta

Received: 14 October 2022

Accepted: 9 November 2022

Published: 15 November 2022

Publisher's Note: MDPI stays neutral with regard to jurisdictional claims in published maps and institutional affiliations.



Copyright: © 2022 by the authors. Licensee MDPI, Basel, Switzerland. This article is an open access article distributed under the terms and conditions of the Creative Commons Attribution (CC BY) license (<https://creativecommons.org/licenses/by/4.0/>).

1. Introduction

Nanomaterials are being studied in a variety of domains, including optoelectronics, biosensors, magnetic sciences, and catalysis. This type of research is developing swiftly. In contrast to other processes, such as chemical synthesis, the biological fabrication of nanomaterials has recently attained popularity because of its simplicity of processing and isolation, ecologically friendly attributes, reusability, and cheap processing cost. The biosynthesized nanoparticles (NPs) are more affordable, durable, and stable than other NPs that are created using traditional techniques [1]. Nanoparticles are used in a variety of processes, including those in the food, medicine, cosmetic, and material engineering industries [2]. Biological methods (so-called “green synthesis”) are promoted as ecofriendly synthesis techniques and include microorganisms, plant extracts, DNA, and proteins. The physicochemical properties of the biosynthesized nanoparticles are similar to those of chemically or physically produced NPs [3].

Zinc and its oxide are among the metals with biological effects that have been extensively investigated. Zinc is an active element with significant chemical properties [4,5]. Due to its bandgap energy and stability, zinc oxide (ZnO) is a viable alternative to titanium

dioxide (TiO₂). Therefore, it has been used in a variety of applications. According to the US Food and Drug Administration, ZnO is a safe food additive [6].

The functionalization of ZnO molecules by bioactive compounds can produce ZnO nanoscale materials with better activity [7]. It is possible to create ZnO nanoparticles by biological, chemical, or physical processes. The synthesis method determines the nanoparticle's crystal formation, shape, size, size distribution, stability, and aggregation characteristics [8]. The most potent microbial killers are nanoparticles made of metals and their oxides, such as Zn, Ag, etc. [2]. Therefore, loading bioactive compounds on metal oxide nanoparticles could boost the activity of metal oxides as antimicrobial agents. Plant extract is employed as a production aid for nanoparticles because it is inexpensive and harmless to the environment. Numerous studies that have used plant extracts to create zinc oxide nanoparticles have been published [3,9–11]. Bacterial infections are considered serious health issues all over the world. The rise in pathogenic strain outbreaks, novel bacterial mutations, and antibiotic resistance have all contributed to the need for the development of more potent antibacterial drugs. We know that zinc oxide has antibacterial characteristics. ZnO nanoparticles are widely recognized to have antibacterial attributes, with activities directly correlated to their concentration, and inversely correlated to their particle size [2].

The antimicrobial action of nanoparticles can target a wide range of strains; nonetheless, their efficacy against different strains can vary significantly. It has previously been established that using ZnO nanoparticles as drugs can affect the growth of fungi, as well as Gram-positive and Gram-negative bacteria. Gram-positive bacteria have a higher sensitivity to ZnO nanoparticles than Gram-negative bacteria [12–14]. The features of the cell wall structure of Gram-negative bacteria can account for their slightly better resistance to antibiotics in particular [15]. ZnO NPs have been investigated as an alternative antibiotic to improve the antibacterial effect against pathogenic strains. They have unique physicochemical characteristics that could affect how microbes react biologically and toxicologically. They primarily work against microbes by releasing metal ions, adsorbing particles, and producing reactive oxygen species [16]. Furthermore, the large specific surface areas of ZnO NPs facilitate adsorption for antimicrobial actions [17]. High antimicrobial efficiency at low concentrations against a variety of bacteria and a comparatively inexpensive cost are only two of the benefits of ZnO nanoparticles. Finding straightforward environmentally friendly techniques to create ZnO nanoparticles with increased antimicrobial properties is thus a crucial and ongoing research challenge [18,19].

Infectious diseases are the leading cause of morbidity in many nations, which is likely due to microbial drug resistance, poverty, and an increase in the unfavorable side effects of antibiotics. These consequences can be solved by developing antimicrobial medicines that originate from plants because they contain a variety of phytochemicals [20]. Several plant extracts, including those of *Hibiscus sabdariffa* L. [21], *Hertia intermedia* [22], *Lavandula stoechas* [23], and *Lavandula angustifolia* [24], have been utilized to functionalize ZnO nanoparticles, which were subsequently assessed for antimicrobial activity. Due to its specific characteristics, such as the use of easily available plants, simplicity, and large variety of ZnO-NP morphologies, subject to the plant extract used, plant-based fabrication is appealing compared with other biological techniques [25]. It has been revealed that lavender plant species have antimicrobial, anti-inflammatory, and antioxidant properties [26–28]; accordingly, people all around the world have long utilized extracts from many species of lavender to cure illnesses, such as migraines, colic pain spasms, etc. [29]. *L. pubescens* shoot methanol extract was found to have potential antimicrobial action [30]. In our study, we fabricated ZnO nanoparticles using zinc chloride solution and *Lavandula pubescens* shoot methanol extract, and we then treated *Staphylococcus aureus* and *Pseudomonas aerogenes* (bacterial strains), and *Aspergillus niger* and *Aspergillus terreus* (fungal strains). We aimed to assess the antimicrobial potential of ZnO nanoparticles dispersed in water and dimethyl sulfoxide (DMSO) by measuring the zone of inhibition (ZI), minimum inhibition concentration (MIC), and minimum bactericidal/fungicide concentration (MBC/MFC).

2. Materials and Methods

2.1. Preparation of *Lavandula pubescens* Shoot Methanol Extract

Lavandula pubescens shoots were collected in Darfur, Sudan. The plant was classified by a botany expert at King Saud University in Riyadh. Shade-dried shoots (moisture content of ~10%) were crushed and then added to a conical flask that previously contained a known volume of 95% methanol (1:10, *w/v*). The flask mixture was shaken for 6 h at room temperature (Wrist Action Shaker, Burrell Scientific, Pittsburgh, PA, USA) after being wrapped in aluminum foil. A rotary evaporator (HAHNVAPOR, HS-2005, Hahn Shin Scientific, Gimpo-si, Korea) was used to reduce the volume of methanol in vacuo. For future usage, the concentrated shoot extractive (66.6 mg/mL) was retained.

2.2. GC–MS Analysis of Compounds in Methanol Extract

The compounds in the *Lavandula pubescens* shoot methanol extract (LPME) were detected by using a gas chromatography (GC) device (Agilent 7890A) combined with a mass spectrometer (5975C, Agilent Technologies, Santa Clara, CA, USA). A DB-5MS GC column (30 m × 0.25 mm inner diameter × 0.25 μm film thickness), Triple-Axis detector, and liquid sampler were included in the GC–MS system. A 22 μm membrane filter was used to filter 1 mL of the extract. The extract was delivered into the system in a 1 μL aliquot. The injection and column temperatures were 280 °C and 300 °C, respectively. The mobile phase was helium (a flow rate of 1 mL/min). We set 70 eV as the electron ionization energy.

2.3. Fabrication of ZnO Nanoparticles

In this experiment, zinc oxide nanoparticles were fabricated as described by the method reported earlier, with some alterations [31]. To prepare a 5 M NaOH solution, 2.5 g of NaOH were added to 12.5 mL of distilled water and stirred (200 rpm). A 2.5 M ZnCl₂ solution was prepared by dissolving 4.2 g of ZnCl₂ in 12.5 mL of distilled water. This solution was gently dropped into the NaOH solution with constant stirring for 30 min at 60 °C, which resulted in the development of a white precipitate (i.e., ZnO particles). After that, 0.75 mL or 1.5 mL of LPME (50 or 100 mg, respectively) was added drop by drop with continuous stirring (200 rpm) at room temperature until the formation of a yellowish color (i.e., ZnO nanoparticles), which ended within 30 min. The prepared nanoparticles were dried in an oven at 60 °C and stored at room temperature for further use. Based on the pretests, 50 mg and 100 mg of LPME were selected for use in the preparation of the LP–ZnO-NP samples (Figure S1).

2.4. Characterization of ZnO Nanoparticles

To assure the formation of ZnO nanoparticles loaded with LPME, we scanned (200–800 nm) the UV–visible spectra (UV-2450 double-beam spectrophotometer, Shimadzu, Tokyo, Japan) of the LPME, ZnO, and LP–ZnO NPs (50 and 100 mg). The X-ray powder diffraction spectra (Bruker D8 Advance diffractometer, Coventry, UK) were scanned to analyze the crystallinity nature of the fabricated nanoparticles. A Cu–K radiation source (1.54 nm; 40 mA; 40 kV) and monochromator were included in the X-ray powder diffractometer. The scanning of the scattered radiations was conducted at 2θ: 10–90° and a 0.02° scan rate. Then, the diffraction patterns of the LPME, ZnO, and LP–ZnO NPs' colloidal solutions were compared with the JCPDS card 36–1451. A Nicolet 6700 Fourier-transform infrared (FT-IR) spectrometer (Waltham, MA, USA) was used to detect the functional groups of the LPME, ZnO₂, and LP–ZnO NPs. The IR-ray scanning was performed at a wavenumber range of 500–4000 cm⁻¹. Microstructural images of nanoparticles were photographed by a transmission electron microscope (TEM) (JEM-1011, JEOL Ltd., Tokyo, Japan), which was worked at 160 kV. A thermal gravimetric analysis (TGA) of the samples was conducted by heating the samples from room temperature to 800 °C (at a heating rate of 10 °C/min) using a thermogravimetric device (Pyris 1 TGA, PerkinElmer, USA).

Before beginning the microbiological assays, the nanoparticles were decontaminated by UV radiation for 10 min. The nanoparticle dilutions were prepared fresh for the experiments.

2.5. Preparation of Tested Bacteria and Fungi

Pseudomonas aeruginosa (ATCC27853) and *Staphylococcus aureus* (ATCC 29213) were donated by the College of Applied Medical Science, King Saud University, and were preserved in nutrient agar (NA) slants. *Aspergillus niger* (ATCC 16404 NA) and *Aspergillus terreus* (ATCC 10029) were obtained from the Mycology Department, King Khalid Hospital, and were inoculated aerobically in Sabouraud dextrose agar (SDA) for 96 h. After collection and preparation, all the organisms were stored for later use at 4 °C.

2.6. In Vitro Antimicrobial Potential of Nanoparticles

2.6.1. Determination of Antimicrobial Activity of ZnO Nanoparticles Loaded with *Lavandula pubescens* Shoot Methanol Extract (50 and 100 mg) Using Agar Well Diffusion Technique

The antimicrobial activities of the LPM, ZnO, and LP-ZnO NPs (50 and 100 mg extracts) were evaluated by the agar well diffusion method. After overnight incubation in nutrient broth, the bacterial suspension turbidity was adjusted to coincide with the 0.5 McFarland standards, followed by the inoculation of the bacteria on a Mueller–Hinton agar (MHA) plate using streaking techniques. To induce sporulation in the fungal strains, a 10-day culture in SDA at 28 °C was used. After submerging in a 5 mL aliquot of sterile 0.85% NaCl (*w/v*), the fungal colonies on the surface were mildly scraped with a sterile loop and transferred to a sterile tube. The fungal inoculum turbidity was standardized as before to obtain a fungal population of 10⁶ CFU (colony-forming units). One milliliter of the fungal suspension previously inoculated was added to SDA and then swabbed onto the surface of the media. Wells of a 6 mm diameter on the agar plates of bacterial and fungal cultures were made using a sterile cork-borer. Then, 7.5 mg of the tested LP-ZnO NPs were added to 1 mL of DMSO/deionized water, followed by sonication. The treating solution (7.5 mg/mL, *w/v*) was applied to the plate wells that had already been inoculated with the studied bacteria/fungi cultures. Augmentin and voriconazole (500 mg/mL) were used as controls (for bacteria and fungi, respectively). After that, the culture plates were left at 4 °C for one hour for the proper diffusion of the nanoparticles [32]. The plates were then incubated for 24 h at 37 °C for the bacteria, and for 7 days at 28 °C for the fungi. The antimicrobial activity was assessed following the incubation period by measuring the zone of inhibition. Every experiment was carried out twice.

2.6.2. The Minimum Inhibitory Concentration (MIC) Assay

For the MIC assay, the broth macrodilution procedure adopted by the Clinical and Laboratory Standards Institute (CLSI) was employed [33]. A total of 1 mL of Mueller–Hinton broth and 1 mL of doubled-concentrated Sabouraud dextrose broth (SDB) were separately added into a tube for the bacteria and fungi, respectively. The tubes were sterilized by an autoclave (121 °C; 15 psi; 30 min). Two-fold serial dilutions were prepared from tube 1 to tube 10 by using the tested LPME, ZnO, and LP-ZnO NP stock solutions in DMSO/deionized water (7.5 mg/mL, *w/v*), while the remaining 1 mL was discarded. Afterward, the standardized inoculum that matches 0.5 McFarland units (from 1 to 2 × 10⁸ CFU/mL) was prepared and then diluted at a ratio of 1:150, which led to a final approximate concentration of 1 × 10⁶ CFU/mL in each tube. Then, 1 mL of the inoculum (1 × 10⁶ CFU/mL) was sequentially added to the serial dilution tubes that contained 1 mL of the broth medium with the tested compound. A tube containing broth inoculated with bacteria/fungi was used as a positive control. This mixture resulted in 1:2 dilutions of the antimicrobial concentrations and a 1:2 dilution of the inoculum. The subsequent 1:2 dilution of the inoculum brought the inoculum concentration to 5 × 10⁵ CFU/mL. To avoid LP-ZnO-NP precipitation, the treated microbial cultures were incubated in a shaking incubator. The incubation of the bacterial cultures lasted 24 h at 37 °C, and the incubation of the fungal cultures lasted 7 days at 28 °C [34].

2.6.3. Minimum Bactericidal/Fungicide Concentration (MBC/MFC) ASSAY

The MBC or MFC refers to the lowest antibiotic concentration that is capable of eradicating at least 99.9% of the microbes. The MBC/MFC were determined using the dilution method of CLSI. The determination of the MBC/MFC was performed by inoculating 0.5 mL of samples that were removed from MIC tubes, with no observed growth, on sterile Mueller–Hinton agar and SDA plates. The plates were then incubated at 37 °C for 24 h for bacteria, and at 28 °C for 7 days for fungi. The concentrations at which no apparent growth was observed were considered the MBC/MFC [35].

2.7. Morphological Examination of Bacterial Cells

The microstructural changes in the bacteria and fungi cells treated with ZnO nanoparticles were observed by a scanning electron microscopy (SEM) device (JEOL model, JSM-7610F, Tokyo, Japan). A total of 1 mL of all tested organism suspensions (10^8 CFU/mL) was mixed with 1 mL of each tested compound, which resulted in a mixture with a 0.5 mg/L concentration. The mixture was then incubated overnight at 37 °C. In a salt-free Lysogeny broth (LB) medium, two controls were prepared: a negative control consisting of an organism and the broth medium, and a positive control consisting of an organism treated with the tested antibiotics and medium. After the incubation, the samples were washed with saline solution and then centrifuged at $1500 \times g$. The samples were fixed with 2.5% glutaraldehyde (4 °C, 2 h), followed by washing with phosphate buffer (pH 7.20). The samples were again fixed in 1% osmium tetroxide, dehydrated using an ascending ethanol series, and then subjected to critical point drying. Finally, the samples were coated with Au–Pd (80:20) using a Polaron E5000 sputter coater, and they were observed on a scanning electron microscope equipped with an SE detector working at 25 kV [36,37].

2.8. Statistical Analysis

The data from three repeated experiments were displayed as means \pm SDs. Data were statistically analyzed using SPSS software, IBM version 20. Multivariate analysis of variance (MANOVA) and ANOVA were used to significantly differentiate between treatment groups. Significant differences between means were determined according to pairwise comparisons (MANOVA) and Tukey's test (ANOVA) at $p < 0.05$.

3. Results and Discussion

3.1. GC–MS Profile of Shoot Methanol Extract of *L. pubescens*

The methanol extract from the *L. pubescens* shoots included a variety of biologically active substances (Table 1; Figure S1). Benzimidazole derivatives of 2-[2-amino-4-methoxyphenyl]benzimidazole (0.24%), for example, have anti-inflammatory properties [38]. A significant component of the methanol shoot extract (21.51%) is indole, 3-(4-nitrophenylamino), and some of its derivatives show anticancer and antibacterial properties against *S. aureus* [39,40]. Methyl nonanoate plays a role as an epitope, antifungal agent, and antinematodal drug [41]. 3-Methyl-4-isopropylphenol and protamine peptide have synergistic antibacterial effects against *Streptococcus mutans* [42]. Synthetic propen-1-one derivatives of 3-(2-benzoxazolylthio)-1-phenyl- Propenone can inhibit cyclooxygenase-2 (COX-2) activity [43]. 2,4-Di-*tert*-butylphenol (3.04%) is an autotoxin with antioxidant properties [44]. Tridecanoic acid, a methyl ester, has an antienteric efficacy against enteropathogenic bacteria, including *Enterococcus faecalis* MCC 2041 T (Gram-positive bacterium) and *Salmonella enterica* serovar Typhimurium MTCC 98 (Gram-negative bacterium) [45]. Diethyl Phthalate causes disturbances to the endocrine system, abnormalities in fetuses, and the dysfunction of the nervous system, and it is also destructive to the environment [46].

Table 1. Chemical compounds of *L. pubescens* methanol shoot extract detected by GC–MS.

No.	RT (min)	Peak Area (%)	Compound Name	Molecular Formula	Molecular Weight (g/mol)	Compound Nature	Bioactivity
1	7.16	0.24	2-[2-Amino-4-methoxyphenyl]benzimidazole	C ₉ H ₁₁ O ₂	165.19	Cyclic aliphatic ketone	Benzimidazole derivatives are anti-inflammatory and anthelmintic agents [38].
2	8.26	21.51	Indole, 3-(4-nitrophenylamino)-	C ₁₄ H ₁₁ N ₃ O ₂	253.26	Heterocyclic organic compound	Its derivatives have anticancer effects [40] and antibacterial effects [39].
3	12.86	0.17	Nonanoic acid, methyl ester (Methyl pelargonate)	C ₁₀ H ₂₀ O ₂	172.26	Fatty acid ester	An epitope, antifungal agent, antineoplastic drug, and plant metabolite [41].
4	14.611	1.76	3-Methyl-4-isopropylphenol	C ₁₀ H ₁₄ O	150.22	Alkylbenzene	It has a synergistic antimicrobial activity against <i>Streptococcus mutans</i> with protamine peptide [42].
5	16.362	0.36	Propenone, 3-(2-benzoxazolylthio)-1-phenyl-	C ₁₆ H ₁₁ NO ₂ S	381.30	Ketone	Synthetic propen-1-one derivatives possess COX-2 inhibitory activity [43].
6	19.103	3.06	2,4-Di-tert-butylphenol	C ₁₄ H ₂₂ O	206.32	Alkylbenzene phenol	A toxic substance and an antioxidant agent [44].
7	19.463	0.10	Tridecanoic acid, methyl ester	C ₁₄ H ₂₈ O ₂	228.37	Fatty acid ester	It has antienteric activity against bacteria [45].
8	20.751	0.18	Diethyl Phthalate	C ₁₂ H ₁₄ O ₄	222.24	Phthalate ester	It is a neurotoxin, teratogenic agent, endocrine disrupter, and harmful to the environment [46].
9	24.59	4.60	1-Nonadecene	C ₁₉ H ₃₈	266.5	Alkene	A bacterial and plant metabolite [47].
10	26.89	0.99	Benzenepropanoic acid, 3,5-bis(1,1-dimethylethyl)-4-hydroxy-, methyl ester (Methyl Di- <i>ter</i> -butyl hydroxyhydrocinnamate)	C ₁₈ H ₂₈ O ₃	292.4	Phenolic acid ester	Its derivatives have antioxidant activities [48].
11	29.60	1.50	9Z,12Z,15Z-Octadecatrien-1-ol	C ₁₈ H ₃₂ O	264.4	Fatty alcohol	An antibacterial agent [49].

Bacteria and plants both produce the metabolite 1-nonadecene (4.60%) [47]. 9Z,12Z,15Z-Octadecatrien-1-ol (1.50%) is an antibacterial agent [48]. Octadecyl-3,5-di-*ter*-butyl-4-hydroxyhydrocinnamate, which is a derivative of methyl di-*ter*-butyl hydroxyhydrocinnamate (0.99%), has antioxidant properties [48,49]. 9Z,12Z,15Z-Octadecatrien-1-ol is an antibacterial agent [48,49].

3.2. ZnO Nanoparticle Characterization Analysis

Figure S3 shows the UV–vis absorption spectra of the LPME, ZnO, and LP–ZnO NPs. ZnO had a broad absorption peak around 374 nm, which was the result of the ZnO π – π^* electronic excitation. The UV–vis band of the 50 mg LP–ZnO NPs was similar to the absorption band of the ZnO, but with higher intensity. The absorption band of the 100 mg LP–ZnO NPs was sharper and slightly shifted to a higher wavelength, which could be a result of the enhancement of the optical properties of the ZnO by the LPME [50]. This led to a shift from the initial solution color (white) to a yellowish color (Figure S2), which is additional proof of a nanosized material production. As can be seen, the 100 mg LP–ZnO NPs displayed a stronger UV band intensity (Figure S3) (i.e., a higher photocatalytic activity) when compared with the 50 mg LP–ZnO NPs [51].

Figure S4 shows the XRD pattern spectra of the ZnO and 50 and 100 mg LP–ZnO NPs. The nanoparticles showed similar characteristic diffraction peaks. The ZnO displayed a broad major band at 31.71° (100), and other minor bands. The nanoparticles showed three major peaks at $2\theta = 31.50^\circ$ (100), 34.19° (002), and 35.99° (101) for the 50 mg LP–ZnO NPs, and 31.50° (100), 34.24° (002), and 36.03° (101) for the 100 mg LP–ZnO NPs. Other minor peaks were also found at 2θ values of 47.28/47.24° (102), 56.25/56.36° (110), 62.68/62.74° (103), 66.02/66.04° (200), 67.75/67.75° (112), 68.89/68.69° (201), 72.28/72.36° (004), 76.68/76.72° (202), 81.09/81.19° (104), and 89.28/89.42° (203) for the 50 and 100 mg LP–ZnO NPs. As can be seen, the nanoparticle peaks conformed to those of the ZnO, which indicates a rod-shaped ZnO crystal structure (Joint Committee on Powder Diffraction Standards (JCPDS) card no. 36–1451), thus confirming the formation of LP–ZnO NPs. Our results were in line with previous research on the green fabrication of ZnO nanoparticles [21,52].

FT-IR analysis was used to determine the organic functional groups that are involved in ZnO-NP biosynthesis (Figure S5). The LPME had a wider band at 3418 cm^{-1} , which was assigned to the O–H stretching vibration of the water, carboxylic acids, and phenolic compounds. The peak appeared at higher wavenumbers of 3435 and 3339 cm^{-1} in the 50 and 100 mg LP–ZnO NPs, respectively. This redshift of the band could be due to the interaction of the O–H groups with Zn ions to form nanoparticles [53]. In the IR spectra of the LPME and LP–ZnO NPs, the bands at 2922 – 2939 cm^{-1} and 2852 – 2859 cm^{-1} conformed to the methylene groups' symmetric and asymmetric stretching vibrations, respectively [54]. The peaks at 1449 – 1521 cm^{-1} in the LPME were related to amide II [55], and they were redshifted after the synthesis of the ZnO nanoparticles. The IR bands at 1382 – 1394 cm^{-1} were related to the C=C stretching of the aromatic amines of the LPME and LP–ZnO NPs. The band related to the C=C stretching of the aromatic amines was blueshifted in the ZnO nanoparticles [21]. In the LPME, the carboxylic-group stretching was reflected by the band at 1597 cm^{-1} , which was redshifted to 1618 – 1627 cm^{-1} after the LP–ZnO-NP synthesis [56]. The bands at 1048 – 1068 cm^{-1} corresponded to C–O stretching vibrations [57]. In the LPME and ZnO nanoparticles, the bands that appeared at 856 – 901 cm^{-1} were ascribed to $-\text{CH}_2$ rocking vibrations [54]. The peaks observed at 477 and 595 cm^{-1} conformed to Zn–O stretching vibrations, and they confirmed the occurrence of ZnO [54].

Figure S6 shows TGA thermograms of the LPME, ZnO, and LP–ZnO NPs. The LPME revealed a three-stage thermogram (Figure S6). The first stage of the extract thermogram at 40 – $200\text{ }^\circ\text{C}$ led to a weight loss of 7.16%, which resulted from the evaporation of water and volatile substances. Furthermore, a significant weight loss (54.60%) was observed at 200 – $600\text{ }^\circ\text{C}$, which was accompanied by an exothermic effect that could be attributed to the ignition of the organic compounds or carbon residues from the previous volatilization. A decomposition stage of two endothermic effects was found at ~ 600 – $775\text{ }^\circ\text{C}$ and $> 775\text{ }^\circ\text{C}$, which led to a loss of $> 93.60\%$ of the initial weight [6,58]. Belardi et al. [58] discovered a minor weight loss (4.45%) of the ZnO precursor at $500\text{ }^\circ\text{C}$, which could be due to the moisture absorption by the hygroscopic Zn ions. A second major weight loss of 45.50% was found at ~ 500 – $800\text{ }^\circ\text{C}$, followed by the pyrolysis of ZnO after heating at $> 800\text{ }^\circ\text{C}$. On the contrary, the 50 and 100 mg LP–ZnO NPs showed a two-stage decomposition with very minimal weight loss, which was due to surface dehydration and dihydroxylation [54]. The 50 mg LP–ZnO NPs exhibited a weight loss of 6.0% at $\sim 740\text{ }^\circ\text{C}$, while the 100 mg LP–ZnO NPs lost 14.5% of their weight at $\sim 700\text{ }^\circ\text{C}$. Similar findings had been reported earlier [54]. The TEM images show the morphology of the biosynthesized ZnO nanoparticles (Figure 1). The synthesized ZnO nanoparticles were agglomerated rods with widths of 10.76 – 20.42 nm for the 50 mg LP–ZnO NPs, and 14.92 – 30.93 nm for the 100 mg LP–ZnO NPs.

3.3. Antimicrobial Properties of ZnO Nanoparticles Loaded with *L. pubescens* Shoot Methanol Extract

3.3.1. The Zone of Inhibition

The zone of inhibition (ZI) monitored the impact of the ZnO nanoparticles loaded with *L. pubescens* shoot methanol extract on the growth of *Staphylococcus aureus*, *Pseudomonas aeruginosa*, *Aspergillus terreus*, and *Aspergillus niger*, which was determined by the agar well diffusion technique. The results are displayed in Table 2, Figures 2a–c and S7. In general, the ZnO and 50 and 100 mg LP–ZnO NPs had good antibacterial and antifungal activities (ZI: 11–24 mm), while the plant extract (LPME) showed the lowest antibacterial and antifungal activities against all the tested microbes, except *S. aureus* (Table 2). Based on the estimated marginal means (Figure 3a), the ZnO showed a higher zone of inhibition (12.88 mm) than the LPME (2.00 mm), irrespective of the type of microbe tested or solvent used. After loading the LPME, the antimicrobial action of the ZnO was improved, as could be seen in the significantly higher zones of inhibition of 13.50 and 12.50 mm for the 50 and 100 mg LP–ZnO NPs, respectively.

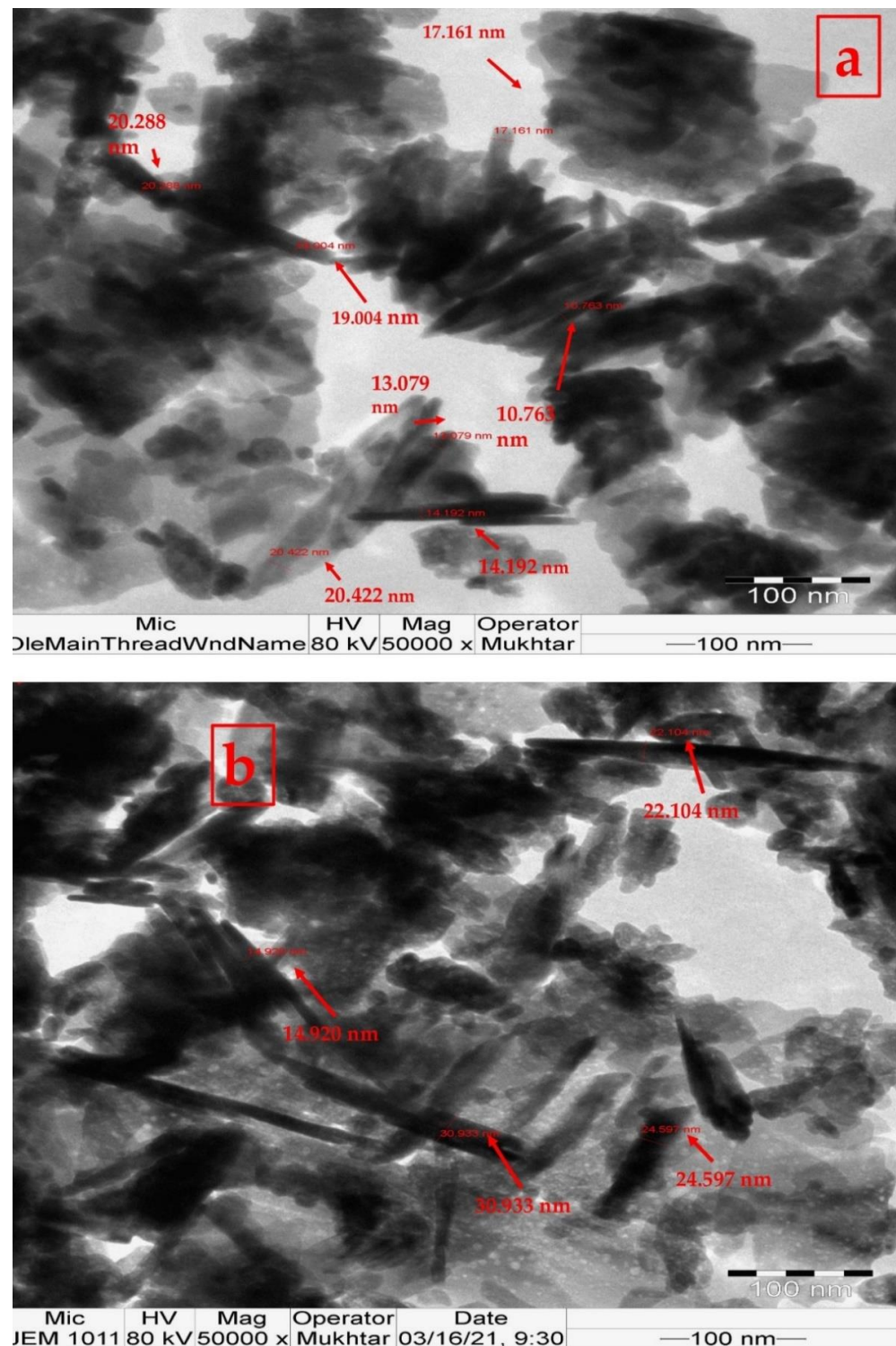


Figure 1. TEM images of Zn oxide nanoparticles prepared by reacting 0.05 M $ZnCl_2$ with *L. pubescens* shoot methanol extract (LPME): (a) 50 mg LPME; (b) 100 mg LPME.

Furthermore, our results indicated that the interaction effects between the microorganisms, solvent type, and ZnO nanoparticles were noticeable (Table 2 and Figure 3a,b). Regarding the role of solvents in the antimicrobial properties of the nanoparticles against the studied bacteria and fungi strains, we noticed a significantly ($p < 0.05$) higher ZI in DMSO (12.25 mm) than in water (8.19 mm) (Figure 2a), which was probably attributed to the higher solubility of the LP-ZnO NPs in DMSO than in water. Despite the lower ZI of

the ZnO nanoparticles in water versus DMSO, it was still significantly higher in the ZnO nanoparticles than that of the control drugs, augmentin/voriconazole, in water (estimated marginal mean of 5.50 mm).

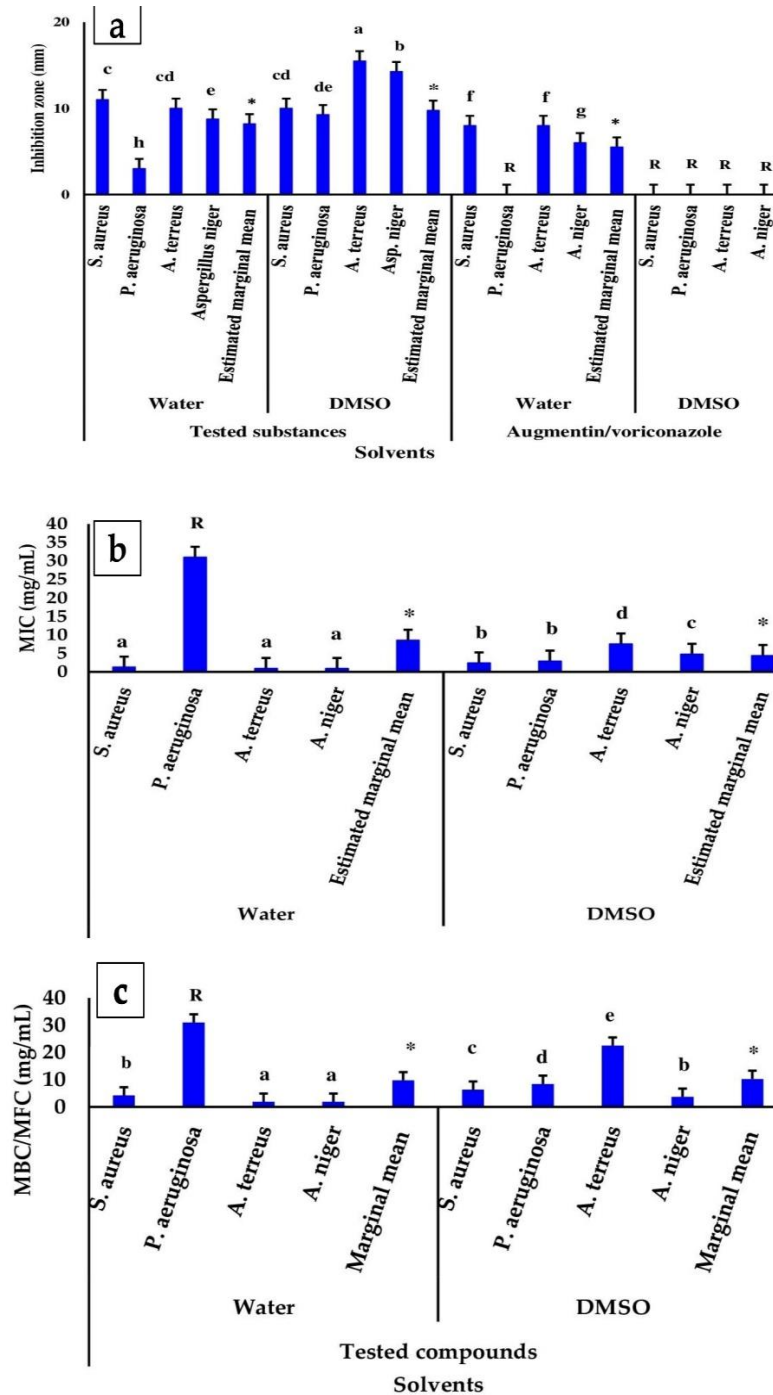


Figure 2. Interaction effects of solvent and microorganisms on microbial activity of ZnO nanoparticles loaded with LPME (50 and 100 mg) (concentration of 7.5 mg/mL): (a): zones of inhibition (ZIs); (b): minimum inhibition concentrations (MICs); (c): minimum bactericidal/fungicide concentrations (MBCs/MFCs). Different letters indicate significant differences between means ($n = 12$) according to pairwise comparisons. (*) indicates significant differences among estimated marginal means ($n = 48$) according to pairwise comparisons. R (>30) refers to an inactive substance or drug-resistant microbe. Augmentin and voriconazole (500 mg/mL) were used as positive controls for bacteria and fungi, respectively. R was given a value of zero for ZI and 31 mg/mL for MIC and MBC/MFC. Bars indicate standard errors of means.

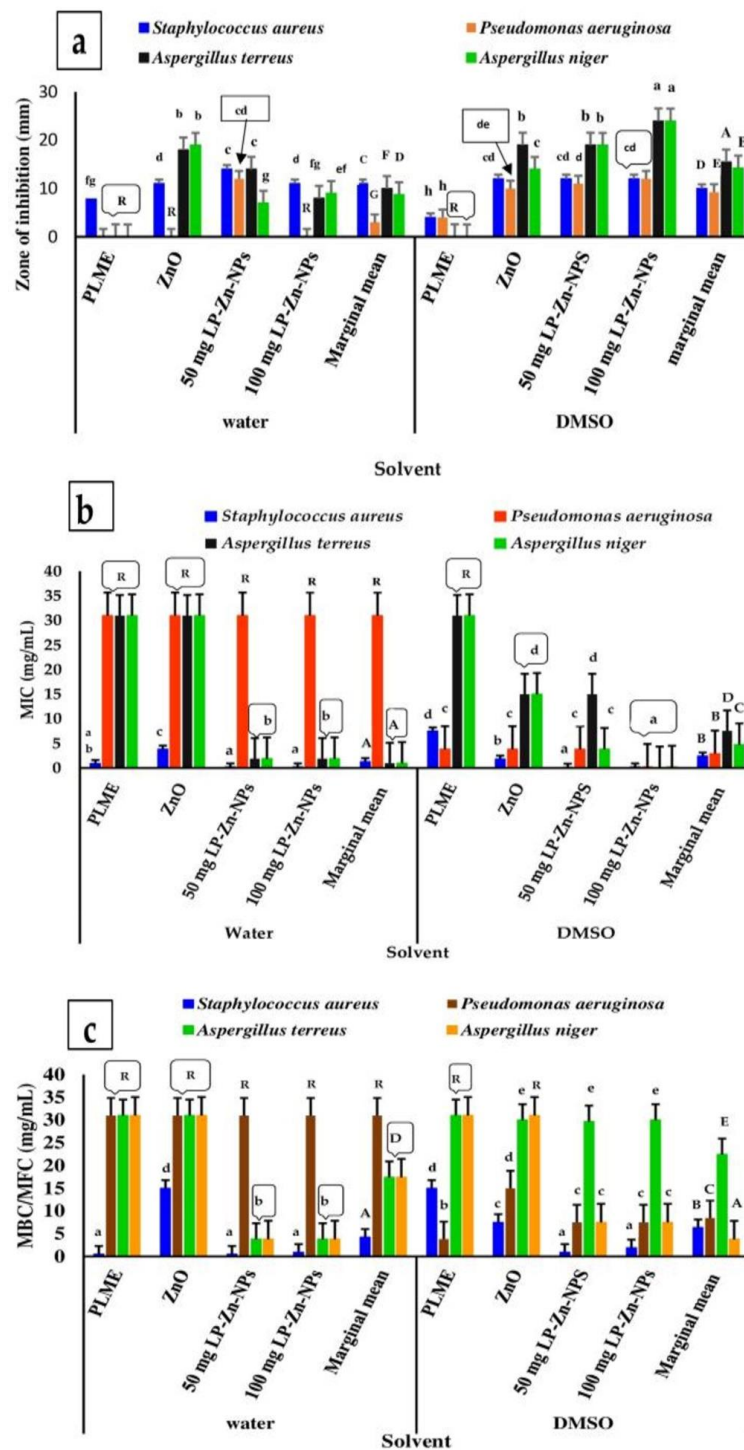


Figure 3. Interaction effects of solvent, microorganisms, and antimicrobial substances (LPME, ZnO, 50 and 100 mg ZnO nanoparticles, with a concentration of 7.5 mg/mL) on microbial activity against tested microbes: (a) ZIs; (b) MICs; (c) MBCs/MFCs. Different uppercase letters indicate significant differences between means ($n = 12$) according to pairwise comparisons. Different lowercase letters indicate significant differences between means ($n = 3$) according to Tukey’s test ($p < 0.05$). R (>30) refers to an inactive substance or drug-resistant microbe. Augmentin and voriconazole (500 mg/mL) were used as positive controls for bacteria and fungi, respectively. R was given a value of zero for ZI and 31 mg/mL for MIC and MBC/MFC. Bars indicate standard errors of means.

When considering how microorganisms, solvents, and treatments interact, the 50 and 100 mg LP–ZnO NPs both showed stronger antifungal efficacy in water than in DMSO

(Figure 2a–c). The highest antimicrobial activity of the 100 mg LP–ZnO NPs was seen in DMSO (Figure 2a–c). Furthermore, the studied ZnO nanoparticles dispersed in the water had significantly lower antifungal activities against *A. terreus* and *A. niger* (inhibition zones of 7 and 14 mm and 8 and 9 mm for 50 and 100 mg LP–ZnO NPs, respectively) when compared with ZnO (Table 2; Figure 2a).

As can be seen from Table 2, the studied bacteria and fungi had significantly varied interactions toward the synthesized ZnO nanoparticles as antimicrobial agents, with ZI marginal means of 10.50, 6.13, 12.5, and 11.5 mm for *Staphylococcus aureus*, *Pseudomonas aeruginosa*, *Aspergillus terreus*, and *Aspergillus niger*, respectively ($p < 0.05$). *Pseudomonas aeruginosa* (a Gram-negative bacterium) was the least affected by the ZnO nanoparticles compared with *Staphylococcus aureus* and the other tested fungi, which suggests that it has a resistance tendency towards ZnO nanoparticles.

3.3.2. Minimum Bactericidal/Fungicide Concentration (MBC/MFC) and Inhibitory Concentration (MIC)

Tables 3 and 4 and Figures 2 and 3 show the MICs and MBCs/MFCs of the ZnO nanoparticles loaded with the *L. pubescens* shoot methanol extract. As can be seen, the MICs and MBCs/MFCs of the 50 mg and 100 mg LP–ZnO NPs were significantly higher (7.22 and 4.88 and 10.59 and 10.81 mg/mL, respectively) compared with those of the LPME and ZnO. Irrespective of the antimicrobial substance used, all the substances showed significantly lower MICs and MBCs/MFCs in water compared with DMSO (Figures 2 and 3). Overall, the MICs of the tested substances against microbes were significantly better in DMSO than in water (estimated marginal means of 4.40 vs. 8.54 mg/mL, respectively) (Figure 2b), while the opposite was true in the case of the MBCs/MFCs, with estimated marginal means of 9.76 and 10.25 mg/mL in water and DMSO, respectively (Figure 2c). In more detail, all the substances had lower MICs and MBCs/MFCs against almost all the tested bacteria and fungi in both water and DMSO, except for *P. aeruginosa* in water, which suggests the higher antimicrobial potential of nanoparticles. It is worth noting that the substances were significantly more active against *S. aureus*, *A. terreus*, and *A. niger* in water than DMSO (Figure 2b,c). The results of the interaction effects of the microorganisms, solvents, and treatments are displayed in Figure 3a–c, which provides a clearer picture of how the tested microbes interacted with the ZnO nanoparticles in water and DMSO. The functionalization of the ZnO by the LPME improved the antibacterial/antifungal activity of the ZnO alone in water and DMSO, which confirmed the inhibition-zone findings. However, the 100 mg LP–ZnO NPs exhibited the highest activity against both bacteria and fungi in DMSO, as seen in the MIC and MBC results (Figure 3b,c). Both the 50 mg and 100 mg LP–ZnO NPs in water had similar antimicrobial effects (Figure 3b,c).

3.3.3. SEM Analysis of ZnO-Nanoparticle-Treated Bacteria and Fungi

The microbial cells treated with the tested substances dissolved in DMSO were photographed by SEM, which was because of the good solubility of ZnO nanoparticles in DMSO. The SEM images of the untreated cells and microbial cells treated with the LPME, 50 mg LP–ZnO NPs, augmentin, and voriconazole are shown in Figures 4 and 5. As can be seen, the treatment of *P. aeruginosa* and *S. aureus* with the LPME and augmentin resulted in minor alterations to the cell surface, with some cells adhering to one another, as seen in Figure 4a–d. The *P. aeruginosa* cell membranes were damaged by the 50 mg LP–ZnO NPs, whereas the *S. aureus* cells showed more severe damage, including pitted, distorted, shriveled, stuck together, and even broken cells. As shown in Figure 5a–g, after receiving 50 mg of the LP–ZnO NPs, the *A. terreus* hyphae developed wrinkles, and the nanoparticles gathered around the vesicles. Similar alterations were observed in the *A. niger* hyphae following treatment with 50 mg of LP–ZnO NPs, but in this case, the vesicles vanished. The *A. terreus* and *A. niger* hyphae did not exhibit any significant alterations in response to the LPME or voriconazole.

Table 2. Zones of inhibition of LPME, ZnO, and LP-ZnO NPs (50 and 100 mg of LPME) against bacteria and fungi.

Microorganism	Zone of Inhibition (Diameter (mm))												Estimated Marginal Mean (n = 24)
	LPME			ZnO			50 mg LP-ZnO NPs			100 mg LP-ZnO NPs			
	Water	DMSO	Total Mean (n = 6)	Water	DMSO	Total Mean (n = 6)	Water	DMSO	Total Mean (n = 6)	Water	DMSO	Total Mean (n = 6)	
<i>Staphylococcus aureus</i>	8.00 ± 0.06	4.00 ± 1.00	6.00 ± 1.30	11.00 ± 0.50	12.00 ± 1.00	11.50 ± 0.89	14.00 ± 0.5	12.00 ± 1.00	13.00 ± 1.30	11.00 ± 0.5	12.00 ± 0.50	11.00 ± 0.71	10.50 ± 3.04 ^d
<i>Pseudomonas aeruginosa</i>	R	4.00 ± 0.50	2.00 ± 0.44	R	10.00 ± 1.00	5.00 ± 11.52	12.00 ± 0.50	11.00 ± 0.50	11.50 ± 0.71	R	12.00 ± 1.00	6.00 ± 3.13	6.13 ± 4.43 ^c
<i>Aspergillus terreus</i>	R	R	R	18.00 ± 0.50	19.00 ± 0.500	18.50 ± 0.71	14.00 ± 1.00	19.00 ± 1.00	16.50 ± 2.88	8.00 ± 1.00	24.00 ± 1.00 ^a	16.00 ± 8.81	12.50 ± 7.62 ^a
<i>Aspergillus niger</i>	R	R	R	19.00 ± 1.00	14.00 ± 1.00	16.50 ± 2.88	7.00 ± 1.00	19.00 ± 1.00	13.00 ± 6.63	9.00 ± 0.50	24.00 ± 0.50	16.50 ± 8.23	11.50 ± 8.73 ^b
Total mean (n = 12)	2.00.00 ± 0.30	2.00 ± 0.21		12.00 ± 5.53	13.75 ± 3.58		11.75 ± 3.06	15.25 ± 4.01		7.00 ± 4.40	18.00 ± 6.30		
Estimated marginal mean (n = 24)			2.00 ± 0.75 ^c			12.88 ± 6.53 ^b			13.50 ± 3.92 ^a			12.50 ± 6.20 ^b	
Grand total mean (n = 96)													10.22 ± 4.24 (SE = 0.072)

The model effects of the multivariate test (Intercept + Treatment + solvent + Microorganism + Treatment * solvent + Treatment * Microorganism + solvent * Microorganism + Treatment * solvent * Microorganism) show a high contribution to the model (significant effects as seen in low Wilks' Lambda values, and high Pillai's trace, Hotelling's trace, and Roy's largest root values of the statistic) (Table S1). The MANOVA tests of the between-subject effects indicate high significant F values. Different letters indicate significant differences ($p < 0.05$) between means according to pairwise comparisons of MANOVA. Univariate test pairwise comparisons indicate significant differences among estimated marginal means of treated groups. R is > 30 mm, which indicates that the compound is inactive, or the microbe is drug resistant. For statistical analysis, R was estimated to be a zero value.

Table 3. Minimum inhibition concentrations (MICs) of LPME, ZnO, and LP–ZnO NPs (50 and 100 mg of LPME) against bacteria and fungi.

Microorganism	MIC (mg/mL)												Estimated Marginal Mean (<i>n</i> = 24)
	LPME			ZnO			50 mg LP–ZnO NPs			100 mg LP–ZnO NPs			
	Water	DMSO	Total Mean (<i>n</i> = 6)	Water	DMSO	Total Mean (<i>n</i> = 6)	Water	DMSO	Total Mean (<i>n</i> = 6)	Water	DMSO	Total Mean (<i>n</i> = 6)	
<i>Staphylococcus aureus</i>	0.90 ± 0.06	7.50 ± 0.80	4.20 ± 2.65	3.80 ± 0.35	1.80 ± 0.15	2.80 ± 1.12	0.20 ± 0.05	0.13 ± 0.03	0.17 ± 0.05	0.20 ± 0.04	0.2 ± 0.00	0.20 ± 0.03	1.84 ± 1.51 ^a
<i>Pseudomonas aeruginosa</i>	R	3.80 ± 0.30	17.40 ± 3.10	R	3.80 ± 0.20	17.40 ± 1.08	R	3.80 ± 0.20	17.40 ± 2.09	R	0.2 ± 0.00	15.60 ± 0.75	16.95 ± 0.80 ^d
<i>Aspergillus terreus</i>	R	R	R	R	15.00 ± 1.00	23.00 ± 3.88	1.90 ± 0.10	15.00 ± 1.30	8.45 ± 1.22	1.90 ± 0.22	0.2 ± 0.00	1.05 ± 0.94	15.87 ± 1.15 ^c
<i>Aspergillus niger</i>	R	R	R	R	15.00 ± 2.00	23.00 ± 2.85	1.90 ± 0.20	3.80 ± 0.4	2.85 ± 1.07	1.90 ± 0.04	0.2 ± 0.00	1.05 ± 0.93	14.48 ± 1.78 ^b
Total mean (<i>n</i> = 12)	23.48 ± 1.16	18.33 ± 2.61		24.20 ± 2.60	8.90 ± 3.50		8.75 ± 0.64	5.68 ± 3.20		8.75 ± 1.54	0.2 ± 0.00		
Estimated marginal mean (<i>n</i> = 24)			20.90 ± 1.43 ^d			16.55 ± 2.09 ^c			7.22 ± 2.01 ^b			4.48 ± 1.17 ^a	
Grand mean (<i>n</i> = 96)													12.29 ± 3.05 (SE = 0.051)

The model effects of the multivariate test (Intercept + Treatment + solvent + Microorganism + Treatment * solvent + Treatment * Microorganism + solvent * Microorganism + Treatment * solvent * Microgm) show a high contribution to the model (significant effects as seen in low Wilks' Lambda values, and high Pillai's trace, Hotelling's trace, and Roy's largest root values of the statistic) (Table S1). The MANOVA of the between-subject effects indicates high significant F values. Different letters indicate significant differences (*p* < 0.05) between means according to pairwise comparisons of MANOVA. R (> 30) refers to inactive compound or resistant microbe. R is > 30 mg/mL. For statistical analysis, R was estimated to be 31 mg/mL.

Table 4. Minimum bactericidal/fungicide concentrations (MBCs/MFCs) of ZnO nanoparticles against bacteria and fungi.

Microorganism	MBC (mg/mL)												Estimated Marginal Mean (n = 24)
	LPME			ZnO			50 mg LP-ZnO NPs			100 mg LP-ZnO NPs			
	Water	DMSO	Total Mean (n = 6)	Water	DMSO	Total Mean (n = 6)	Water	DMSO	Total Mean (n = 6)	Water	DMSO	Total Mean (n = 6)	
<i>Staphylococcus aureus</i>	0.50 ± 0.10	15.00 ± 1.00	7.75 ± 1.90	15.00 ± 1.30	7.50 ± 0.50	11.25 ± 3.42	0.50 ± 0.10	0.90 ± 0.30	0.70 ± 0.30	0.90 ± 0.20	1.90 ± 0.26	1.40 ± 0.59	5.28 ± 4.17 ^a
<i>Pseudomonas aeruginosa</i>	R	3.80 ± 0.10	17.40 ± 1.62	R	15.00 ± 0.50	23.00 ± 2.77	R	7.50 ± 1.90	19.25 ± 1.93	R	7.50 ± 0.90	19.25 ± 2.73	19.73 ± 2.30 ^b
<i>Aspergillus terreus</i>	R	R	R	R	30.00 ± 2.00	30.50 ± 1.78	3.80 ± 0.00	29.67 ± 0.58	16.73 ± 4.48	3.80 ± 0.20	30.00 ± 1.00	16.90 ± 4.66	23.78 ± 7.15 ^c
<i>Aspergillus niger</i>	R	R	R	R	0.00 ± 0.00	31.00 ± 0.00	3.80 ± 0.07	7.50 ± 0.50	5.65 ± 2.05	3.80 ± 0.30	7.50 ± 0.30	5.65 ± 2.04	18.33 ± 1.02 ^b
Total mean (n = 12)	23.38 ± 3.08	20.20 ± 4.31		27.00 ± 4.86	20.88 ± 4.51		9.78 ± 0.88	11.39 ± 11.62		9.88 ± 1.70	11.73 ± 5.29		
Estimated marginal mean (n = 24)			21.79 ± 4.62 ^c			23.94 ± 4.35 ^b			10.59 ± 2.03 ^a			10.81 ± 1.96 ^a	
Grand mean (n = 96)													16.78 ± 3.09 (SE = 0.067)

The model effects of the multivariate test (Intercept + Treatment + solvent + Microorganism + Treatment * solvent + Treatment * Microorganism + solvent * Microorganism + Treatment * solvent * Microgm) show a high contribution to the model (significant effects as seen in low Wilks' Lambda values, and high Pillai's trace, Hotelling's trace, and Roy's largest root values of the statistic) (Table S1). The MANOVA of the between-subject effects indicates high significant F values. Different letters indicate significant differences ($p < 0.05$) between means according to pairwise comparisons of MANOVA. R (> 30) refers to inactive compound or resistant microbe. R is > 30 mg/mL. For statistical analysis, R was estimated to be 31 mg/mL.

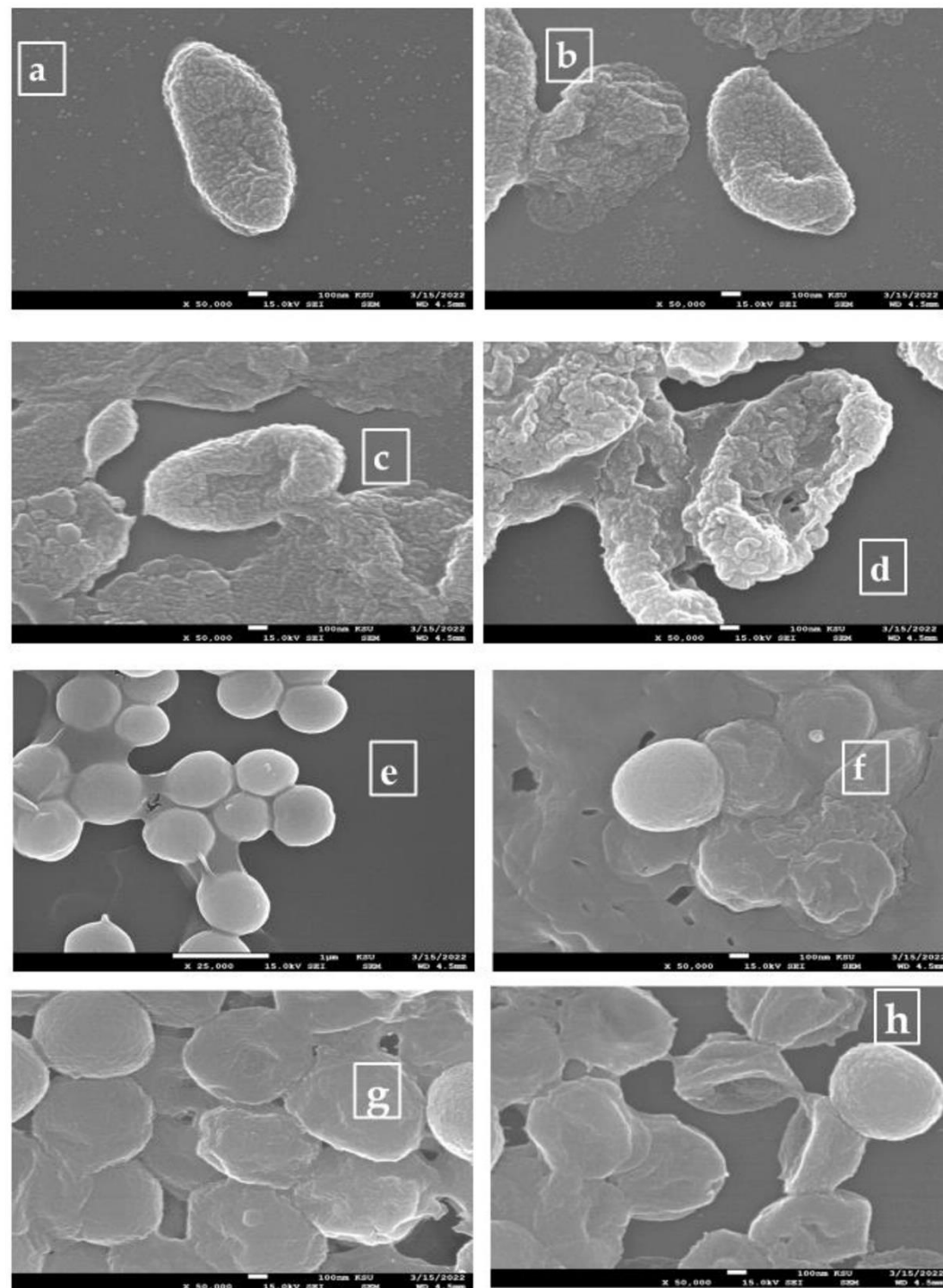


Figure 4. SEM images of *Pseudomonas aeruginosa* cells: (a) normal cells; (b–d) cells treated with augmentin, LPME, and 50 mg LP-ZnO NPs, respectively. SEM images of *Staphylococcus aureus* cells: (e) normal cells; (f–h) cells treated with augmentin, LPME, and 50 mg LP-ZnO NPs, respectively. DMSO was used as a solvent.

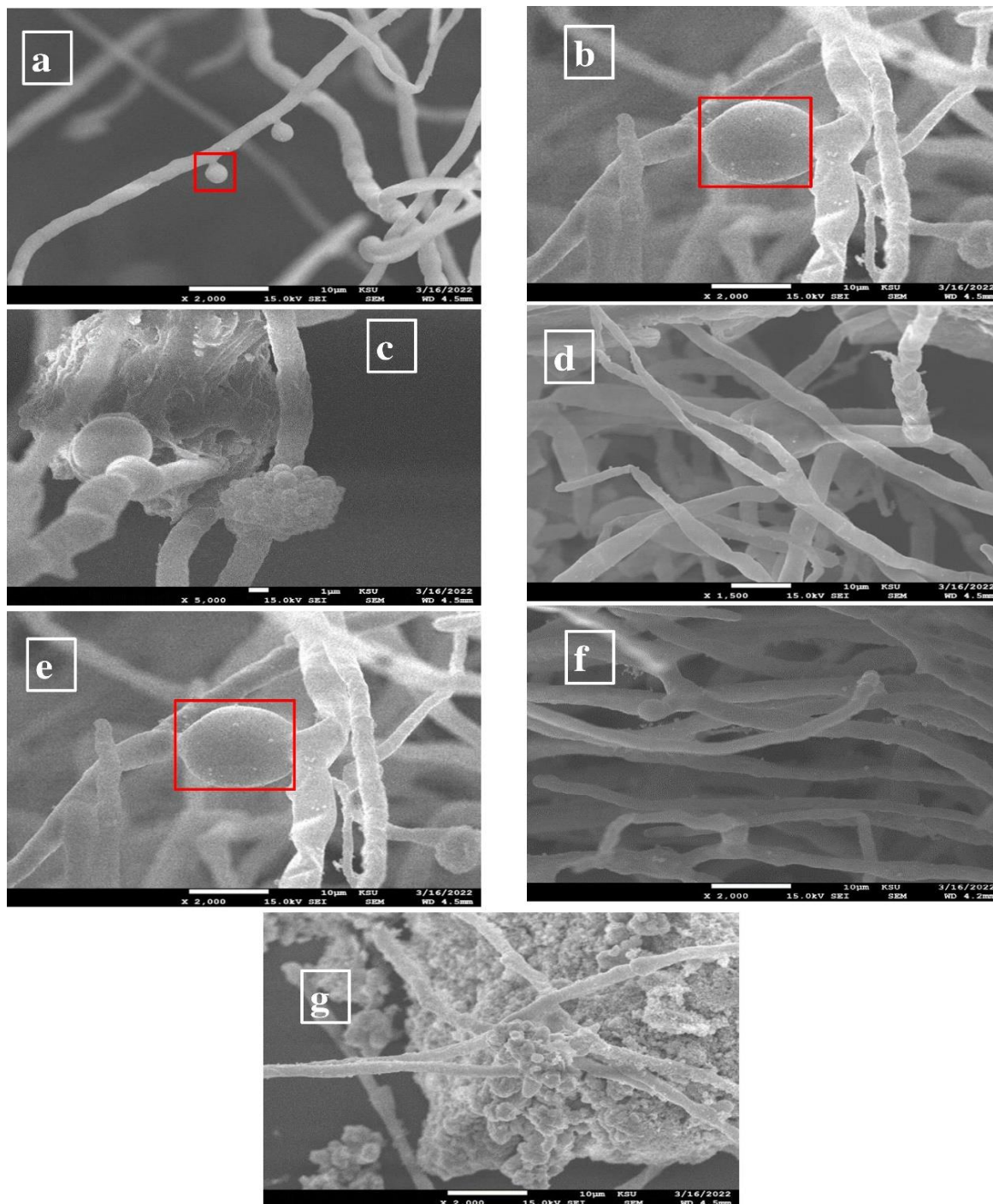


Figure 5. SEM images of *Aspergillus terreus* cells: (a) normal cells; (b,c) cells treated with voriconazole and 50 mg LP-ZnO NPs, respectively. SEM images of *Aspergillus niger*: (d) normal cells; (e–g): cells treated with voriconazole, LPME, and 50 mg LP-ZnO NPs, respectively. DMSO was used as a solvent. Red squares indicate normal vesicles.

4. Discussion

Due to the widespread usage of nanoscale metals in industries such as food, medicine, and the environment, synthesizing these materials is currently a hot research topic. The majority of metal nanoparticles are produced chemically, which has unforeseen consequences, such as energy and environmental waste, as well as potential health risks. It is essential to discover a method of synthesizing ZnO NPs that is safe for the environment and uses gentle processes and nontoxic components. Green synthesis, which reduces metal ions using

plant extracts rather than synthetic chemicals, was created in response to these difficulties. Green synthesis has several benefits: it is affordable and nonhazardous to human health and the environment [59,60]. Recently, researchers have become interested in the utilization of biomaterials for the manufacture of ZnO NPs. Plant, fungal, bacterial, algal, arthropod, enzyme, animal, and agricultural waste products are all examples of biomaterials. Because of some characteristics, such as the use of easily available plants, simplicity, and the wide range of ZnO-NP morphologies, the manufacture of plant-based ZnO nanoparticles is preferable to alternative biological methods [25].

Plants are fascinating sources of different bioactive substances, such as alkaloids, flavonoids, saponins, steroids, tannins, etc. These natural secondary metabolites are found in the plant parts, including the roots, shoots, leaves, flowers, stems, bark, fruits, and seeds; thus, they serve as a reducing and stabilizing agent during the synthesis of metallic nanoparticles [61]. Lavender is one of the most fashionable aromatic medicinal plants in the world [62]. Flavonoids are primarily *Lavandula*-species-specific compounds that are explored for their ability to significantly increase the plasma superoxide dismutase and glutathione peroxidase activities while also reducing the malondialdehyde levels. They also demonstrate significant anti-inflammatory activity and cytotoxicity against Bel-7402 and Hela cells [29] (Zhao et al., 2015). These bioactivities have verified the traditional usage of this plant, which is worth developing and studying. In our research, we analyzed the composition of the methanol shoot extract of *Lavandula pubescens* using the GC-MS device. *Lavandula pubescens* contains vital bioactive compounds other than flavonoids with antimicrobial and antioxidant activities, such as indole, 3-(4-nitrophenylamino) [39,40], methyl nonanoate [41], 3-methyl-4-isopropylphenol [42], 2,4-Di-*tert*-butylphenol [44], and tridecanoic acid, methyl ester [45]. Due to its exceptional abilities in optics, electronics, and photonics, and its affordability, high catalytic efficiency, wide-band-gap energy, large exciton-binding energy, and high potential to adsorb UV-light irradiation, ZnO has attracted significant scientific interest as a substitute for TiO₂. The efficacy of the photocatalytic reactions in ZnO is constrained by the quick recombination of the photoexcited electron-hole pairs. In actuality, the recombination process significantly lowers the quantum efficiency of photocatalysis, and it has faster kinetics than surface redox processes [63].

One of the more alluring biological processes is the plant-mediated synthesis of ZnO nanoparticles owing to characteristics such as the viability, use of readily available plants, and wide array of ZnO-nanoparticle morphologies that result from the variations in the plant bioactive compounds [64]. During the fabrication of the LP-ZnO-NP samples, the compounds of the *Lavandula pubescens* shoot methanol extract were used as a reducing agent to develop ZnO NPs, and their formation, as well as structural features, were evaluated by UV-vis, XRD, and TEM. We next investigated the antimicrobial capabilities of the LP-ZnO NPs against *P. aeruginosa* (Gram-negative bacterium) and *S. aureus* (Gram-positive bacterium), *A. niger*, *A. terreus*, and *Staphylococcus aureus*. The presence of the ZnO main XRD band and FT-IR band in the manufactured nanoparticles, as well as the functionalization of the ZnO by the LPME compounds as reducing and capping agents, ascertained that the functionalization led to nanosized agglomerated LP-ZnO NP rods (Figure S4, Figure 1). Additionally, the production of the nanosized LP-ZnO NPs was indicated by the broadening of the (101) diffraction peaks [53]. Regarding our FT-IR results (Figure S5), we observed changes in the intensity or shifts in the positions of the IR bands of the LPME after the fabrication of the ZnO nanoparticles, which suggested that the bioactive compounds bonded to the ZnO surface. It has been reported that the bioactive compounds present in plant extracts, such as polyphenols (flavonoids), have hydroxyl and ketonic groups that bind to bulk metal oxide to reduce it to a nanosize [65]. In more detail, LPME carboxylic acids and phenolic compounds probably interact with ZnO, as evidenced by the appearance of C-O functional groups in nanoparticles [21,54]. These findings confirmed the functionalization of ZnO nanoparticles as well. The high thermal stability of ZnO nanoparticles (Figure S6), with the stability higher in the 50 mg LP-ZnO NPs than 100 mg LP-ZnO NPs, conforms to the finding reported earlier [4]. This suggests

that these nanoparticles can be used as antimicrobial additives in the food industry. The biofabrication of ZnO nanoparticles from plants and their use as antimicrobial agents have been extensively investigated by many authors [25,51,66]. ZnO NPs have been investigated as an alternative antibiotic to improve the antibacterial effect against pathogenic strains. They have unique physicochemical characteristics that might affect how bacteria react biologically and toxicologically. They primarily work against microbes by releasing metal ions, adsorbing particles, and producing reactive oxygen species [16].

Furthermore, we went through the physicochemical characteristics of the synthesized LP-ZnO NPs so that we could understand how effective they are against harmful microbes, and specifically the effect of the *L. pubescens* shoot methanol extract on the growth of *Staphylococcus aureus* (Gram-positive bacterium), *Pseudomonas aeruginosa* (Gram-negative bacterium), *Aspergillus terreus*, and *Aspergillus niger*. To combat the multidrug resistance, scientists have looked at zinc oxide nanoparticles for use in developing next-generation nano-antibiotics against pathogenic bacteria [3,67]. The agar well diffusion approach was used to detect the inhibitory zones (ZIs) of the tested microbes created by the fabricated LP-ZnO NPs, which indicated the antimicrobial potential of the LP-ZnO NPs. Next, using the broth microdilution method, the minimum inhibitory concentrations (MICs) and minimum bactericidal/fungicidal concentrations (MBCs/MFCs) of the LP-ZnO NPs were determined.

We noticed that the growth behavior of the tested bacteria and fungi after the ZnO nanoparticle treatment varied depending on the type of microbe, the antimicrobial substance's qualities, and the type of solvent (Table 2 and Figure 2a–c). The biofabricated ZnO nanoparticles improved the antimicrobial performance of the ZnO alone, which resulted from the reduction in the ZnO by reactive substances (Figure S5), which were probably adsorbed onto the molecule surface from the LPME, with the generation of reactive oxygen species, such as hydrogen peroxide radicals, superoxide radicals, etc.; thus, they induce apoptosis by the internalization of the hydrogen peroxide radicals or the loss of the cellular integrity following the interaction between ZnO NPs and the cell wall [68]. Biologically fabricated ZnO nanoparticles gain two benefits that result from the biological functionalization: high biocompatibility and decreased microbial drug resistance [69]. Based on the estimated marginal means (Figure 3a), after loading the LPME, the antimicrobial action of the ZnO was improved, which was the result of the biofunctionalization by the *L. pubescens* methanol extract, which contains compounds with antimicrobial properties (Section 3.1).

We observed the interaction effects between the microorganisms, solvent type, and ZnO nanoparticles (Table 2 and Figure 3a,b) (i.e., how the examined strains of bacteria and fungi responded to the antimicrobial activities of the nanoparticles in various solvents). We observed that the ZI was higher in DMSO than in water (Figure 2a), which was probably attributable to the higher solubility of the LP-ZnO NPs in DMSO than in water. Interestingly, the antibacterial activity of the 50 mg LP-ZnO NPs in water against *S. aureus* and *P. aeruginosa* was significantly better than that of the 100 mg LP-ZnO NPs (Figure 2a). This could be the result of the good biofunctionalization and smaller particle size of the synthesized 50 mg LP-ZnO NPs, which was ascertained by the aforementioned characterization findings (Section 3.2). The 50 and 100 mg LP-ZnO NPs both showed stronger antifungal efficacy in water than in DMSO (Figure 2a–c), which might be because the ZnO nanoparticles dispersed in water could promote ROS, and especially H₂O₂ radicals, which are capable of internalizing the cell and causing apoptosis. In this regard, Lipovsky et al. [70] examined ZnO NPs as an antifungal agent against *Candida albicans*, and they proposed that the generation of ROS might be the factor that led to the fungal apoptosis in the aqueous medium. The antimicrobial activity of ZnO alone in DMSO, but not in water, was enhanced by functionalizing the nanoparticles with *L. pubescens* shoot extract (Figure 2a–c). The ZnO surface may physically adsorb the bioactive compounds found in LPME, thus reducing and capping the ZnO to produce functionalized LP-ZnO NPs. Markham et al. [71] concluded that, after the crystal loses a photoexcited electron to O₂, organic compounds, such as phenolate and alcoholate anions adsorbed onto the zinc oxide surface, are oxidized either by the transfer of the electrons to the photopositive zinc oxide surface, or through the

absorption of hydrogen by the peroxide radical. The broadening of the inhibition zone for diverse bacteria reflects the species-sensitive nature of the cytotoxic impact of a particular metal oxide nanoparticle [72]. Despite the lower ZIs of the ZnO nanoparticles in water versus DMSO, they were still significantly higher in the ZnO nanoparticles than in the control drugs, augmentin/voriconazole, in water. In this study, the alterations noticed in the inhibitory zones after the bacterial and fungi cultures were exposed to the biosynthesized LP-ZnO-NP treatments could be due to the enhancement of the ZnO by the LPME bioactive compounds adsorbed onto its surface. The LPME, as a functionalizing material, demonstrated antimicrobial potential, such as indole, 3-(4-nitrophenylamino), which has anticancer and antibacterial properties against *S. aureus* [39,40]; nonanoic acid, methyl ester, which is an antifungal agent [41]; 3-methyl-4-isopropylphenol, which has synergistic antibacterial effects against *Streptococcus mutans* [42]; tridecanoic acid, methyl ester, which has antienteric efficacy against enteropathogenic bacteria, such as *Enterococcus faecalis* (Gram-positive bacterium) and *Salmonella enterica* (Gram-negative bacterium) [45].

The cell cytotoxicity required direct particle–cell interaction, and the toxicity of the particles was unrelated to the concentration of the soluble ZnO under the cell growth conditions. One of the factors behind cell death is the disruption of the mitochondrial function. Strong indications of apoptosis, the loss of the mitochondrial potential, and an increase in ROS generation were observed in the cells exposed to ZnO particulate matter. However, when the cells were exposed to a similar quantity of a soluble Zn salt, these signs were not present. There was a statistically significant increase in the potency per unit mass with the smaller particles compared with the larger particles, even though both ZnO samples produced similar toxicity mechanisms [73]. Nevertheless, there are concerns about the toxicity of nanoparticles under 100 nm in comparison with larger particles of the same substance [73]. However, zinc oxide nanoparticles selectively harm bacteria while having little effect on human and animal tissues. Additionally, zinc is recognized as an essential trace element for the physiological and biochemical processes in humans and animals. Therefore, the Food and Drug Administration has approved the use of zinc as a food additive [12,74].

According to our results (Table 2), the studied bacteria and fungi had significantly varied interactions toward the synthesized ZnO nanoparticles as antimicrobial agents, with varied ZI marginal means. *Pseudomonas aeruginosa* (Gram-negative bacterium) was the microbe that was the least affected by the ZnO nanoparticles, compared with *Staphylococcus aureus* and the other tested fungi, which suggests that it had a resistance tendency towards ZnO nanoparticles. ZnO NPs have the capability of inhibiting the growth of both Gram-positive and Gram-negative bacteria, as well as that of fungi. The sensitivity of the bacteria determines the strength of the antimicrobial impact [75]. A thick film of peptidoglycan (20–80 nm) makes up the cell wall of Gram-positive bacteria, acting as a physical barrier to safeguard the surroundings of the cell. Teichoic and lipoteichoic acids, as well as surface proteins, are polymers that are fixed by this thick layer of peptidoglycan. Gram-negative bacteria have highly complex cell walls [68,76]. According to Tayel and colleagues [77], Gram-positive bacteria are more vulnerable to ZnO-nanoparticle attacks than Gram-negative bacteria. The antibacterial attributes of zinc oxide nanoparticles have been shown to be directly proportional to their concentration and particle surface area [78]. However, ZnO nanoparticles have the potential to alter the environment around bacteria by creating ROS or by modifying the cell wall of the microbe as a result of the electrostatic binding of the ZnO nanoparticles to the cell surface, which can lead to cellular destruction [79,80]. Because it immediately lowers the amount of oxygen in the water, some bacteria have cytochrome oxidase, which can interfere with the antibacterial effects of ZnO nanoparticles. *P. aeruginosa* has strong drug resistance because it produces both catalase and cytochrome oxidase, which enable bacteria to scavenge hydrogen peroxide radicals [68,81]. Because of their unique characteristics, such as their crystallinity, porosity, and particle size and shape, ZnO NPs are capable of inhibiting a wide variety of pathogens, including *Escherichia coli*, *Staphylococcus aureus*, *Pseudomonas aeruginosa*, *Bacillus subtilis*, etc. [82,83]. Reactive

oxygen species (ROS)-based photocatalytic antimicrobial interactions under ultraviolet (UV) and visible light irradiation are also enhanced by the intra- and interparticle pores of ZnO NPs [3]. A cell membrane's ability to adsorb ZnO nanoparticles for antibacterial activities is also facilitated by their high specific surface areas [17].

Research authors [84,85] have conclusively reported that ZnO NPs exhibit antibacterial activity, depending on the concentration and surface area, because more H₂O₂ radicals can be created on the surfaces of ZnO nanoparticles. Increases in the nanoparticle concentration and surface area can lead to increased antibacterial activity. It is believed that H₂O₂ radicals can permeate the cell membranes of bacteria, cause damage, and restrict cell growth because the bacterial cell membrane is relatively permeable to them [86]. Moreover, it was demonstrated that the antibacterial activity of ZnO NPs could occur even in the dark, which indicates the possibility of the presence of other mechanisms apart from those that require UV irradiation for the production of ROS in the absence of light. The negatively charged bacterial cell [87,88] allows strong electrostatic binding between the nanoparticles and bacterium surface, thus producing cell membrane damage that leads to the leakage of the intracellular content [89,90]. Our SEM image (Figures 4 and 5) showed the adherence of the LP-ZnO NPs to the microbial cell surfaces.

Furthermore, our research findings revealed that all the tested substances had lower MICs and MBCs/MFCs against almost all the tested bacteria and fungi in both water and DMSO, except for *P. aeruginosa* in water, which suggests the higher antimicrobial potential of nanoparticles. It is worth noting that the examined antimicrobial substances were significantly more active against *S. aureus*, *A. terreus*, and *A. niger* in water than DMSO (Figure 2). A clearer picture of how the tested microbes interacted with the ZnO nanoparticles in water and DMSO can be seen in the fact that the 100 mg LP-ZnO NPs exhibited the highest activity against both bacteria and fungi in DMSO, as seen in the MIC and MBC results. Both the 50 mg and 100 mg LP-ZnO NPs in water had similar antimicrobial effects (Figure 3). Meanwhile, *S. aureus* was the most susceptible microbe to damage by the tested antimicrobial substances, while *P. aeruginosa* was the least. In other words, the Gram-positive *S. aureus* requires a lower MIC, versus the higher MIC required for Gram-negative *P. aeruginosa*. The ability to create specific compounds that boost their resistance to oxidative stress is inherent to Gram-negative bacteria [82]. *S. aureus*, which is a food-producing enterotoxin bacterium, is primarily responsible for most food poisoning cases and a multitude of foodborne illnesses. It shares with other bacteria the extraordinary capacity to withstand the administration of any antibiotic [5]. Similar results from previous research on Gram-positive and Gram-negative bacteria have already been reported [91,92]. Furthermore, the tested nanoparticles showed higher effect sizes on the MICs and MBCs/MFCs than on the ZIs (Table S2). Our findings concluded that the activity of the synthesized LP-ZnO NPs was more potent than those of commercial antibiotics, such as augmentin and voriconazole, and that it was influenced by the solvent type and microorganism type. The SEM imaging of the tested bacteria and fungi strains after the LP-ZnO-NP treatment showed alterations to and damage on the cell wall surface, which confirms the antimicrobial potency of the studied ZnO nanoparticles (Figures 4 and 5). This was noticed in the severe damage to the cell membranes of all the tested microbes, and especially *P. aeruginosa*, *A. niger*, and *S. aureus*. The inadequacy of DMSO as a solvent for augmentin and voriconazole could adversely affect their antimicrobial activities. Wang et al. [69] reported similar distortions in the cell membrane of *S. aureus* with an accumulation of ZnO nanoparticles. Our SEM findings conformed to those reported previously on bacteria and fungi [93–95]. Eskandari et al. [96] demonstrated that ZnO nanorods have both fungicide and fungistatic action against *Candida albicans*, which is consistent with our MFC and SEM results. ZnO nanoparticles can be used with anti-inflammatory drugs and antibiotics to boost the antimicrobial action against pathogenic bacteria without developing antibiotic resistance in nonclinical and clinical settings [86]. Our findings concluded that the activity of the synthesized LP-ZnO NPs was more potent than those of commercial antibiotics, such as augmentin and voriconazole, and that it was influenced by the solvent type and microorganism type.

5. Conclusions

In the present study, we demonstrated that ZnO nanoparticles loaded with *L. pubescens* shoot methanol extract exhibited good antimicrobial effects on both bacteria (*P. aeruginosa* and *S. aureus*) and fungi (*A. niger* and *A. terreus*). Loading the ZnO oxide nanoparticles with the shoot methanol extract enhanced their antimicrobial activity, with higher ZIs, lower MICs, and MBCs/MFCs. Overall, the antimicrobial activity of the LP–ZnO NPs (50 and 100 mg) in DMSO against the fungi, and particularly against the tested bacteria, was better than in water. Despite this, the 50 mg LP–ZnO NPs in water had a superior antibacterial impact on *S. aureus* and *P. aeruginosa*. The SEM images proved the antimicrobial potential of the LP–ZnO NPs through the observed changes in the microbial cell surfaces, and they provided a preliminary view of the mechanism of action of ZnO nanoparticles. According to the findings, the prepared LP–ZnO NPs are a promising alternative for treating a wide array of microbes due to their advantage in preventing microbial growth, which is better than antibiotics.

Supplementary Materials: The following are available online at: <https://www.mdpi.com/article/10.3390/app122211613/s1>. Figure S1. Chemical compounds of *L. pubescens* methanol shoot extract detected by GC–MS; Figure S2. *Lavandula pubescens* shoot methanol extract, ZnO, and ZnO nanoparticle emulsion solutions (50 mg extract + 0.05 M ZnCl₂ and 100 mg extract + 0.05 M ZnCl₂); Figure S3. UV–vis spectra of ZnO and LP–ZnO NPs prepared by reacting 50 mg and 100 mg of *L. pubescens* shoot methanol extract (LPME) with 0.05 M ZnCl₂ solution; Figure S4. XRD spectra. Zinc oxide (a); zinc oxide NPs prepared by reacting 0.05 M ZnCl₂ with 50 mg (b) and 100 mg (c) of *L. pubescens* shoot methanol extract; Figure S5. FT-IR spectra: extract (a); zinc oxide (b); zinc oxide NPs prepared by reacting 0.05 M ZnCl₂ with 50 mg (c) and 100 mg (d) of *L. pubescens* shoot methanol extract; Figure S6. Thermogravimetric curves of tested antimicrobial compounds: LPME (*L. pubescens* shoot methanol extract); ZnO₂ (zinc oxide); 50 mg and 100 mg LP–ZnO NPs (zinc oxide nanoparticles prepared using 50 and 100 mg of the methanol extract, respectively); Figure S7. Zone of inhibition of ZnO nanoparticles loaded with *Lavandula pubescens* shoot methanol extract (LPME) (50 mg and 100 mg LP–ZnO NPs; concentration: 7.5 mg/mL) against *Pseudomonas aeruginosa* (a); *Staphylococcus aureus* (b,c); *Aspergillus niger* (d,e); *Aspergillus terreus* (f). Controls: augmentin/voriconazole (concentration: 500 mg/mL); LPME (concentration: 7.5 mg/mL); Table S1. Multivariate tests^a for zone of inhibition, minimum inhibition concentration, and minimum bactericidal or fungicide concentration; Table S2. Effect size[#] of treatments (LPME, ZnO, LP–ZnO NPs) on ZIs, MICs, and MBCs of tested bacteria and fungi.

Author Contributions: A.E.A.Y., project administration, conceptualization, software, writing—original draft, editing, and review; G.M.A.-S., supervision; L.N.A.-H., supervision; P.S.-B., methodology; M.A.M., methodology, software; R.E., methodology, writing—original draft; M.A.Y., S.Z.A.F., resources, data curation. All authors have read and agreed to the published version of the manuscript.

Funding: The research was funded by the Researchers Supporting Project, King Saud University, Riyadh, Saudi Arabia, grant number RSP-2021/84.

Institutional Review Board Statement: There are no animal or human objects used in this study. So, delete this section.

Informed Consent Statement: Not applicable.

Data Availability Statement: The data presented in this study are available in the article or Supplementary Materials.

Acknowledgments: The authors extend their appreciation to the Researchers Supporting Project, King Saud University, Riyadh, Saudi Arabia, grant number RSP-2021/84.

Conflicts of Interest: The authors declare no conflict of interest regarding this paper.

References

1. Rasli, N.I.; Basri, H.; Harun, Z. Zinc oxide from aloe vera extract: Two-level factorial screening of biosynthesis parameters. *Heliyon* **2020**, *6*, e03156. [CrossRef] [PubMed]
2. Siddiqi, K.S.; Husen, A. Properties of zinc oxide nanoparticles and their activity against microbes. *Nanoscale Res. Lett.* **2018**, *13*, 1–13. [CrossRef] [PubMed]

3. Jin, S.-E.; Jin, H.-E. Synthesis, characterization, and three-dimensional structure generation of zinc oxide-based nanomedicine for biomedical applications. *Pharmaceutics* **2019**, *11*, 575. [[CrossRef](#)] [[PubMed](#)]
4. Sawai, J. Quantitative evaluation of antibacterial activities of metallic oxide powders (ZnO, MgO, and CaO) by conductimetric assay. *J. Microbiol. Methods* **2003**, *54*, 177–182. [[CrossRef](#)]
5. Maret, W. Metals on the move: Zinc ions in cellular regulation and in the coordination dynamics of zinc proteins. *Biometals* **2011**, *24*, 411–418. [[CrossRef](#)]
6. Zare, E.; Pourseyedi, S.; Khatami, M.; Darezereshki, E. Simple biosynthesis of zinc oxide nanoparticles using nature's source, and it's in vitro bio-activity. *J. Mol. Struct.* **2017**, *1146*, 96–103. [[CrossRef](#)]
7. Fatimah, I.; Pradita, R.Y.; Nurfalinda, A. Plant extract mediated of ZnO nanoparticles by using ethanol extract of *Mimosa pudica* leaves and coffee powder. *Procedia Eng.* **2016**, *148*, 43–48. [[CrossRef](#)]
8. Król, A.; Pomastowski, P.; Rafińska, K.; Railean-Plugaru, V.; Buszewski, B. Zinc oxide nanoparticles: Synthesis, antiseptic activity and toxicity mechanism. *Adv. Colloid Interface Sci.* **2017**, *249*, 37–52. [[CrossRef](#)]
9. Ifeanyichukwu, U.L. Omolola Esther Fayemiand Collins Njie Ateba. Green Synthesis of Zinc Oxide Nanoparticles from Pomegranate (*Punica granatum*) Extracts and Characterization of Their Antibacterial Activity. *Molecules* **2020**, *25*, 4521. [[CrossRef](#)]
10. Abdallah, Y.; Liu, M.; Ogunyemi, S.O.; Ahmed, T.; Fouad, H.; Abdelazez, A.; Yan, C.; Yang, Y.; Chen, J.; Li, B. Bioinspired Green Synthesis of Chitosan and Zinc Oxide Nanoparticles with Strong Antibacterial Activity against Rice Pathogen *Xanthomonas oryzae* pv. *Oryzae*. *Molecules* **2020**, *25*, 4795. [[CrossRef](#)]
11. Alyamani, A.A.; Albukhaty, S.; Aloufi, S.; AlMalki, F.A.; Al-Karagoly, H.; Sulaiman, G.M. Green Fabrication of Zinc Oxide Nanoparticles Using *Phlomis* Leaf Extract: Characterization and In Vitro Evaluation of Cytotoxicity and Antibacterial Properties. *Molecules* **2021**, *26*, 6140. [[CrossRef](#)] [[PubMed](#)]
12. Yusof, N.A.A.; Zain, N.M.; Pauzi, N. Synthesis of ZnO nanoparticles with chitosan as stabilizing agent and their antibacterial properties against Gram-positive and Gram-negative bacteria. *Int. J. Biol. Macromol.* **2019**, *124*, 1132–1136. [[CrossRef](#)] [[PubMed](#)]
13. Gudkov, S.V.; Burmistrov, D.E.; Serov, D.A.; Rebezov, M.B.; Semenova, A.A.; Lisitsyn, A.B. A mini review of antibacterial properties of ZnO nanoparticles. *Front. Phys.* **2021**, *9*, 641481. [[CrossRef](#)]
14. Zhong, L.; Liu, H.; Samal, M.; Yun, K. Synthesis of ZnO nanoparticles-decorated spindle-shaped graphene oxide for application in synergistic antibacterial activity. *J. Photochem. Photobiol. B Biol.* **2018**, *183*, 293–301. [[CrossRef](#)] [[PubMed](#)]
15. Kashef, N.; Huang, Y.-Y.; Hamblin, M.R. Advances in antimicrobial photodynamic inactivation at the nanoscale. *Nanophotonics* **2017**, *6*, 853–879. [[CrossRef](#)]
16. El-Masry, R.M.; Talat, D.; Hassoubah, S.A.; Zabermaawi, N.M.; Eleiwa, N.Z.; Sherif, R.M.; Mohammed, A.S.; Abourehab, M.A.S.; Abdel-Sattar, R.M.; Gamal, M.; et al. Evaluation of the Antimicrobial Activity of ZnO Nanoparticles against Enterotoxigenic *Staphylococcus aureus*. *Life* **2022**, *12*, 1662. [[CrossRef](#)]
17. de Lucas-Gil, E.; Leret, P.; Monte-Serrano, M.; Reinoso, J.J.; Enríquez, E.; Del Campo, A.; Cañete, M.; Menéndez, J.; Fernández, J.F.; Rubio-Marcos, F. ZnO Nanoporous Spheres with Broad-Spectrum Antimicrobial Activity by Physicochemical Interactions. *ACS Appl. Nano Mater.* **2018**, *1*, 3214–3225. [[CrossRef](#)]
18. Agarwal, H.; Shanmugam, V. A review on anti-inflammatory activity of green synthesized zinc oxide nanoparticle: Mechanism-based approach. *Bioorg. Chem.* **2020**, *94*, 103423. [[CrossRef](#)]
19. Alamdari, S.; Sasani Ghamsari, M.; Lee, C.; Han, W.; Park, H.-H.; Tafreshi, M.J.; Afarideh, H.; Ara, M.H.M. Preparation and characterization of zinc oxide nanoparticles using leaf extract of *Sambucus ebulus*. *Appl. Sci.* **2020**, *10*, 3620. [[CrossRef](#)]
20. Shaikh, I.A.; Muddapur, U.M.; Bagewadi, Z.K.; Chiniwal, S.; Ghoneim, M.M.; Mahnashi, M.H.; Alsaikhan, F.; Yaraguppi, D.; Niyonzima, F.N.; More, S.S.; et al. Characterization of Bioactive Compounds from *Acacia concinna* and *Citrus limon*, Silver Nanoparticles' Production by *Acacia concinna* Extract, and Their Biological Properties. *Molecules* **2022**, *27*, 2715. [[CrossRef](#)]
21. Bala, N.; Saha, S.; Chakraborty, M.; Maiti, M.; Das, S.; Basu, R.; Nandy, P. Green synthesis of zinc oxide nanoparticles using *Hibiscus subdariffa* leaf extract: Effect of temperature on synthesis, anti-bacterial activity and anti-diabetic activity. *RSC Adv.* **2015**, *5*, 4993–5003. [[CrossRef](#)]
22. Soltanian, S.; Sheikhabaei, M.; Mohamadi, N.; Pabarja, A.; Abadi, M.F.S.; Tahroudi, M.H.M. Biosynthesis of zinc oxide nanoparticles using *Hertia intermedia* and evaluation of its cytotoxic and antimicrobial activities. *BioNanoScience* **2021**, *11*, 245–255. [[CrossRef](#)]
23. Yilmaz, D.; Fatih, D.; Onmaz, N. Comparison of antimicrobial activity of bio-synthesized silver and zinc oxide nanoparticles using *Lavandula stoechas* leaf extract. *Res. J. Biotechnol.* **2019**, *14*, 24–29.
24. Rather, G.A.; Nanda, A.; Raj, E.; Mathivanan, N.; Nayak, B. Green synthesis of ZnO nanoparticles using the leaf extract of *Lavandula angustifolia* and evaluation of their antibacterial activity against human pathogens. *Int. J. Health Sci.* **2022**, *6*, 13478–13485. [[CrossRef](#)]
25. Pillai, A.M.; Sivasankarapillai, V.S.; Rahdar, A.; Joseph, J.; Sadeghfar, F.; Rajesh, K.; Kyzas, G.Z. Green synthesis and characterization of zinc oxide nanoparticles with antibacterial and antifungal activity. *J. Mol. Struct.* **2020**, *1211*, 128107. [[CrossRef](#)]
26. Turgut, A.C.; Emen, F.M.; Canbay, H.S.; Demirdöğen, R.E.; Çam, N.; Kılıç, D.; Yeşilkaynak, T. Chemical characterization of *Lavandula angustifolia* Mill. as a phytocosmetic species and investigation of its antimicrobial effect in cosmetic products. *J. Turk. Chem. Soc. Sect. A Chem.* **2017**, *4*, 283–298. [[CrossRef](#)]
27. Yassine Ez zoubi, Y.; Boust, D.; Abdellah Farah, A. A Phytopharmacological review of a Mediterranean plant: *Lavandula stoechas* L. *Clin. Phytosci.* **2020**, *6*, 9. [[CrossRef](#)]

28. Hawrył, A.; Hawrył, M.; Waksmundzka-Hajnos, M. Liquid chromatography fingerprint analysis and antioxidant activity of selected lavender species with chemometric calculations. *PLoS ONE* **2019**, *14*, e0218974. [[CrossRef](#)]
29. Zhao, J.; Xu, F.; Huang, H.; Ji, T.; Li, C.; Tan, W.; Chen, Y.; Ma, L. Evaluation on bioactivities of total flavonoids from *Lavandula angustifolia*. *Pak. J. Pharm. Sci.* **2015**, *28*, 1245–1251.
30. Mousa, O.; Gouda, B.; Salama, M.; El-Eraky, W.; Kassem, H. Total phenolic, total flavonoid content, two isolates and bioactivity of *Lavandula pubescens* Decne. *Int. J. Pharmacogn. Phytochem. Res.* **2018**, *10*, 254–263.
31. Divya, B.; Karthikeyan, C.; Rajasimman, M. Chemical synthesis of zinc oxide nanoparticles and its application of dye decolourization. *Int. J. Nanosci. Nanotechnol.* **2018**, *14*, 267–275.
32. Richardson, P.M.; Harborne, J.B. *Phytochemical Methods: A Guide to Modern Techniques of Plant Analysis*. Second Edition. *Brittonia* **1990**, *42*, 115. [[CrossRef](#)]
33. Wayne, P. Reference method for broth dilution antifungal susceptibility testing of yeasts. *Clin. Lab. Stand. Inst.* **2008**, *3*, M27-A23.
34. Pereira, F.d.O.; Wanderley, P.A.; Viana, F.A.C.; Lima, R.B.d.; Sousa, F.B.d.; Lima, E.d.O. Growth inhibition and morphological alterations of *Trichophyton rubrum* induced by essential oil from *Cymbopogon winterianus* Jowitt ex Bor. *Braz. J. Microbiol.* **2011**, *42*, 233–242. [[CrossRef](#)]
35. Alekish, M.; Ismail, Z.B.; Albiss, B.; Nawasrah, S. In vitro antibacterial effects of zinc oxide nanoparticles on multiple drug-resistant strains of *Staphylococcus aureus* and *Escherichia coli*: An alternative approach for antibacterial therapy of mastitis in sheep. *Vet. World* **2018**, *11*, 1428. [[CrossRef](#)]
36. Liu, S.; Long, Q.; Xu, Y.; Wang, J.; Xu, Z.; Wang, L.; Zhou, M.; Wu, Y.; Chen, T.; Shaw, C. Assessment of antimicrobial and wound healing effects of Brevinin-2Ta against the bacterium *Klebsiella pneumoniae* in dermally-wounded rats. *Oncotarget* **2017**, *8*, 111369. [[CrossRef](#)]
37. Sharma, N.; Singh, V.; Pandey, A.K.; Mishra, B.N.; Kulsoom, M.; Dasgupta, N.; Khan, S.; El-Enshasy, H.A.; Haque, S. Preparation and evaluation of the ZnO NP–ampicillin/sulbactam nanoantibiotic: Optimization of formulation variables using RSM coupled GA method and antibacterial activities. *Biomolecules* **2019**, *9*, 764. [[CrossRef](#)]
38. Veerasamy, R.; Roy, A.; Karunakaran, R.; Rajak, H. Structure–activity relationship analysis of benzimidazoles as emerging anti-inflammatory agents: An overview. *Pharmaceuticals* **2021**, *14*, 663. [[CrossRef](#)]
39. Khedr, F.; Ibrahim, M.K.; Eissa, I.H.; Abulkhair, H.S.; El-Adl, K. Phthalazine-based VEGFR-2 inhibitors: Rationale, design, synthesis, in silico, ADMET profile, docking, and anticancer evaluations. *Arch. Pharm.* **2021**, *354*, 2100201. [[CrossRef](#)]
40. Devi, N.; Kaur, K.; Biharee, A.; Jaitak, V. Recent Development in Indole Derivatives as Anticancer Agent: A Mechanistic Approach. *Anti Cancer Agents Med. Chem.* **2021**, *21*, 1802–1824. [[CrossRef](#)]
41. CHEBI:44499. Methyl Nonanoate. Available online: <https://www.ebi.ac.uk/chebi/searchId.do?chebiId=CHEBI:44499> (accessed on 7 August 2022).
42. CHEBI:34429. 3-Methyl-4-Isopropylphenol. Available online: <https://www.ebi.ac.uk/chebi/searchId.do?chebiId=CHEBI:34429> (accessed on 7 August 2022).
43. Arfaie, S.; Zarghi, A. Design, synthesis and biological evaluation of new (E)- and (Z)-1, 2, 3-triaryl-2-propen-1-ones as selective COX-2 inhibitors. *Eur. J. Med. Chem.* **2010**, *45*, 4013–4017. [[CrossRef](#)] [[PubMed](#)]
44. CHEBI:89188. 2,4-Di-tert-butylphenol. Available online: <https://www.ebi.ac.uk/chebi/searchId.do?chebiId=CHEBI:89188> (accessed on 7 August 2022).
45. Misra, D.; Ghosh, N.N.; Mandal, M.; Mandal, V.; Baildya, N.; Mandal, S. Anti-enteric efficacy and mode of action of tridecanoic acid methyl ester isolated from *Monochoria hastata* (L.) Solms leaf. *Braz. J. Microbiol.* **2022**, *53*, 715–726. [[CrossRef](#)] [[PubMed](#)]
46. CHEBI:34698. Diethyl Phthalate. Available online: <https://www.ebi.ac.uk/chebi/searchId.do?chebiId=CHEBI:34698> (accessed on 7 August 2022).
47. CHEBI:64503. 1-Nonadecene. Available online: <https://www.ebi.ac.uk/chebi/searchId.do?chebiId=CHEBI:64503> (accessed on 7 August 2022).
48. Saunier, J.; Mazel, V.; Paris, C.; Yagoubi, N. Polymorphism of Irganox 1076[®]: Discovery of new forms and direct characterization of the polymorphs on a medical device by Raman microspectroscopy. *Eur. J. Pharm. Biopharm.* **2010**, *75*, 443–450. [[CrossRef](#)] [[PubMed](#)]
49. CHEBI:77474. 9Z,12Z,15Z-Octadecatrien-1-ol. Available online: <https://www.ebi.ac.uk/chebi/searchId.do?chebiId=CHEBI:77474> (accessed on 7 August 2022).
50. Krishnamoorthy, R.; Athinarayanan, J.; Periyasamy, V.S.; Alshuniaber, M.A.; Alshammari, G.; Hakeem, M.J.; Ahmed, M.A.; Alshatwi, A.A. Antibacterial Mechanisms of Zinc Oxide Nanoparticle against Bacterial Food Pathogens Resistant to Beta-Lactam Antibiotics. *Molecules* **2022**, *27*, 2489. [[CrossRef](#)] [[PubMed](#)]
51. Santhoshkumar, J.; Kumar, S.V.; Rajeshkumar, S. Synthesis of zinc oxide nanoparticles using plant leaf extract against urinary tract infection pathogen. *Resour.-Effic. Technol.* **2017**, *3*, 459–465. [[CrossRef](#)]
52. Talam, S.; Karumuri, S.R.; Gunnam, N. Synthesis, characterization, and spectroscopic properties of ZnO nanoparticles. *Int. Sch. Res. Netw.* **2012**, *2012*, 372505. [[CrossRef](#)]
53. Ismail, M.; Taha, K.; Modwi, A.; Khezami, L. ZnO nanoparticles: Surface and X-ray profile analysis. *J. Ovonic Res.* **2018**, *14*, 381–393.
54. Dinesh, V.; Biji, P.; Ashok, A.; Dhara, S.; Kamruddin, M.; Tyagi, A.; Raj, B. Plasmon-mediated, highly enhanced photocatalytic degradation of industrial textile dyes using hybrid ZnO@Ag core–shell nanorods. *RSC Adv.* **2014**, *4*, 58930–58940. [[CrossRef](#)]

55. Alshammari, G.M.; Yagoub, A.E.A.; Subash-Babu, P.; Hassan, A.B.; Al-Nouri, D.M.; Mohammed, M.A.; Yahya, M.A.; Elsayim, R. Inhibition of lipid accumulation and adipokine levels in maturing adipocytes by bauhinia rufescens (lam.) stem bark extract loaded titanium oxide nanoparticles. *Molecules* **2021**, *26*, 7238. [[CrossRef](#)]
56. Manrique, G.D.; Lajolo, F.M. FT-IR spectroscopy as a tool for measuring degree of methyl esterification in pectins isolated from ripening papaya fruit. *Postharvest Biol. Technol.* **2002**, *25*, 99–107. [[CrossRef](#)]
57. Wei, Y.; Zhang, L.; Yu, Z.; Lin, K.; Yang, S.; Dai, L.; Liu, J.; Mao, L.; Yuan, F.; Gao, Y. Enhanced stability, structural characterization and simulated gastrointestinal digestion of coenzyme Q10 loaded ternary nanoparticles. *Food Hydrocoll.* **2019**, *94*, 333–344. [[CrossRef](#)]
58. Belardi, G.; Ballirano, P.; Ferrini, M.; Lavecchia, R.; Medici, F.; Piga, L.; Scoppettuolo, A. Characterization of spent zinc–carbon and alkaline batteries by SEM-EDS, TGA/DTA and XRPD analysis. *Thermochim. Acta* **2011**, *526*, 169–177. [[CrossRef](#)]
59. Guan, Z.; Ying, S.; Ofoegbu, P.C.; Clubb, P.; Rico, C.; He, F.; Hong, J. Green synthesis of nanoparticles: Current developments and limitations. *Environ. Technol. Innov.* **2022**, *26*, 102336. [[CrossRef](#)]
60. Bhardwaj, B.; Singh, P.; Kumar, A.; Kumar, S.; Budhwa, V. eco-friendly greener synthesis of nanoparticles. *Adv. Pharm. Bull.* **2020**, *10*, 566–576. [[CrossRef](#)]
61. Sorbiun, M.; Mehr, E.S.; Ramazani, A.; Malekzadeh, A.M. Biosynthesis of metallic nanoparticles using plant extracts and evaluation of their antibacterial properties. *Nanochem. Res.* **2018**, *3*, 1–16. [[CrossRef](#)]
62. Parkash, V.; Singh, H. *Lavandula angustifolia* L. (Lavender): An important aromatic medicinal shrub and its in vitro micro-propagation for conservation. *Int. Agric. Technol.* **2013**, *9*, 691–702.
63. Vaiano, V.; Matarangolo, M.; Murcia, J.J.; Rojas, H.; Navío, J.A.; Hidalgo, M.C. Enhanced photocatalytic removal of phenol from aqueous solutions using ZnO modified with Ag. *Appl. Catal. B Environ.* **2018**, *225*, 197–206. [[CrossRef](#)]
64. Agarwal, H.; Kumar, S.V.; RajeshKumar, S. A review on green synthesis of zinc oxide nanoparticles- An ecofriendly approach. *Resour.-Effic. Technol.* **2017**, *3*, 406–413. [[CrossRef](#)]
65. Abdelkader, D.H.; Negm, W.A.; Elekhrawy, E.; Eliwa, D.; Basmah, N.; Aldosari, B.N.; Alanood, S.; Almurshedi, A.S. Zinc oxide nanoparticles as potential delivery carrier: Green synthesis by *Aspergillus niger* endophytic fungus, characterization, and in vitro/in vivo antibacterial activity. *Pharmaceuticals* **2022**, *15*, 1057. [[CrossRef](#)]
66. Lingaraju, K.; Raja Naika, H.; Manjunath, K.; Basavaraj, R.B.; Nagabhushana, H.; Nagaraju, G.; Suresh, D. Biogenic synthesis of zinc oxide nanoparticles using *Ruta graveolens* (L.) and their antibacterial and antioxidant activities. *Appl. Nanosci.* **2016**, *6*, 703–710. [[CrossRef](#)]
67. Makabenta, J.M.V.; Nabawy, A.; Li, C.-H.; Schmidt-Malan, S.; Patel, R.; Rotello, V.M. Nanomaterial-based therapeutics for antibiotic-resistant bacterial infections. *Nat. Rev. Microbiol.* **2021**, *19*, 23–36. [[CrossRef](#)] [[PubMed](#)]
68. da Silva, B.L.; Caetano, B.L.; Chiari-Andréo, B.G.; Pietro, R.C.L.R.; Chiavacci, L.A. Increased antibacterial activity of ZnO nanoparticles: Influence of size and surface modification. *Colloids Surf. B. Biointerfaces* **2019**, *177*, 440–447. [[CrossRef](#)] [[PubMed](#)]
69. Wang, D.; Cui, L.; Chang, X.; Guan, D. Biosynthesis and characterization of zinc oxide nanoparticles from *Artemisia annua* and investigate their effect on proliferation, osteogenic differentiation of zinc oxide nanoparticles in human osteoblast-like MG-63 cells. *J. Photochem. Photobiol. B Biol.* **2020**, *202*, 111652. [[CrossRef](#)] [[PubMed](#)]
70. Lipovsky, A.; Nitzan, Y.; Gedanken, A.; Lubart, R. Antifungal activity of ZnO nanoparticles—The role of ROS mediated cell injury. *Nanotechnology* **2011**, *22*, 105101. [[CrossRef](#)]
71. Markham, M.C.; Hannan, M.C.; Paternostro, R.M.; Rose, C.B. Oxidation of alcohols catalyzed by zinc oxide and light. *J. Am. Chem. Soc.* **1958**, *80*, 5394–5397. [[CrossRef](#)]
72. Baek, Y.-W.; An, Y.-J. Microbial toxicity of metal oxide nanoparticles (CuO, NiO, ZnO, and Sb₂O₃) to *Escherichia coli*, *Bacillus subtilis*, and *Streptococcus aureus*. *Sci. Total Environ.* **2011**, *409*, 1603–1608. [[CrossRef](#)]
73. Moose, P.J.; Chung, K.; Woessner, D.; Honegger, M.; Cutler, N.S.; Veranth, J.M. ZnO particulate matter requires cell contact for toxicity in human colon cancer cells. *Chem. Res. Toxicol.* **2010**, *23*, 733–739. [[CrossRef](#)]
74. Namvar, F.; Rahman, H.S.; Mohamad, R.; Azizi, S.; Tahir, P.M.; Chartrand, M.S.; Yeap, S.K. Cytotoxic effects of biosynthesized zinc oxide nanoparticles on murine cell lines. *Evid.-Based Complement. Altern. Med.* **2015**, *2015*, 593014. [[CrossRef](#)]
75. Bhattacharyya, S.; Majhi, S.; Saha, B.P.; Mukherjee, P.K. Chlorogenic acid–phospholipid complex improve protection against UVA induced oxidative stress. *J. Photochem. Photobiol. B Biol.* **2014**, *130*, 293–298. [[CrossRef](#)]
76. Leung, Y.; Chan, C.; Ng, A.; Chan, H.; Chiang, M.; Djurišić, A.; Ng, Y.; Jim, W.; Guo, M.; Leung, F. Antibacterial activity of ZnO nanoparticles with a modified surface under ambient illumination. *Nanotechnology* **2012**, *23*, 475703. [[CrossRef](#)]
77. Tayel, A.A.; El-Tras, W.F.; Moussa, S.; El-Baz, A.F.; Mahrous, H.; Salem, M.F.; Brimer, L. Antibacterial action of zinc oxide nanoparticles against foodborne pathogens. *J. Food Saf.* **2011**, *31*, 211–218. [[CrossRef](#)]
78. Raghupathi, K.R.; Koodali, R.T.; Manna, A.C. Size-dependent bacterial growth inhibition and mechanism of antibacterial activity of zinc oxide nanoparticles. *Langmuir* **2011**, *27*, 4020–4028. [[CrossRef](#)] [[PubMed](#)]
79. Heinlaan, M.; Ivask, A.; Blinova, I.; Dubourguier, H.-C.; Kahru, A. Toxicity of nanosized and bulk ZnO, CuO and TiO₂ to bacteria *Vibrio fischeri* and crustaceans *Daphnia magna* and *Thamnocephalus platyurus*. *Chemosphere* **2008**, *71*, 1308–1316. [[CrossRef](#)] [[PubMed](#)]
80. Hajipour, M.J.; Fromm, K.M.; Ashkarran, A.A.; de Aberasturi, D.J.; de Larramendi, I.R.; Rojo, T.; Serpooshan, V.; Parak, W.J.; Mahmoudi, M. Antibacterial properties of nanoparticles. *Trends Biotechnol.* **2012**, *30*, 499–511.

81. Pasquet, J.; Chevalier, Y.; Couval, E.; Bouvier, D.; Noizet, G.; Morlière, C.; Bolzinger, M.-A. Antimicrobial activity of zinc oxide particles on five micro-organisms of the Challenge Tests related to their physicochemical properties. *Int. J. Pharm.* **2014**, *460*, 92–100. [[CrossRef](#)]
82. da Silva, B.L.; Abuçafy, M.P.; Berbel Manaia, E.; Oshiro Junior, J.A.; Chiari-Andréo, B.G.; Pietro, R.C.R.; Chiavacci, L.A. Relationship between structure and antimicrobial activity of zinc oxide nanoparticles: An overview. *Int. J. Nanomed.* **2019**, *14*, 9395–9410. [[CrossRef](#)]
83. Sánchez-López, E.; Gomes, D.; Esteruelas, G.; Bonilla, L.; Lopez-Machado, A.L.; Galindo, R.; Cano, A.; Espina, M.; Ettcheto, M.; Camins, A.; et al. Metal-based nanoparticles as antimicrobial agents: An overview. *Nanomaterials* **2020**, *10*, 292. [[CrossRef](#)]
84. Jalal, R.; Goharshadi, E.K.; Abareshi, M.; Moosavi, M.; Yousefi, A.; Nancarrow, P. ZnO nanofluids: Green synthesis, characterization, and antibacterial activity. *Mater. Chem. Phys.* **2010**, *121*, 198–201. [[CrossRef](#)]
85. Padmavathy, N.; Vijayaraghavan, R. Enhanced bioactivity of ZnO nanoparticles—An antimicrobial study. *Sci. Technol. Adv. Mat.* **2008**, *9*, 035004. [[CrossRef](#)]
86. Rokbani, H.; Daigle, F.; Aji, A. Combined effect of ultrasound stimulations and autoclaving on the enhancement of antibacterial activity of ZnO and SiO₂/ZnO nanoparticles. *Nanomaterials* **2018**, *8*, 129. [[CrossRef](#)]
87. Stoimenov, P.K.; Klinger, R.L.; Marchin, G.L.; Klabunde, K.J. Metal oxide nanoparticles as bactericidal agents. *Langmuir* **2002**, *18*, 6679–6686. [[CrossRef](#)]
88. Hirota, K.; Sugimoto, M.; Kato, M.; Tsukagoshi, K.; Tanigawa, T.; Sugimoto, H. Preparation of zinc oxide ceramics with a sustainable antibacterial activity under dark conditions. *Ceram. Int.* **2010**, *36*, 497–506. [[CrossRef](#)]
89. Zhang, L.; Jiang, Y.; Ding, Y.; Povey, M.; York, D. Investigation into the antibacterial behaviour of suspensions of ZnO nanoparticles (ZnO nanofluids). *J. Nanopart. Res.* **2007**, *9*, 479–489. [[CrossRef](#)]
90. Xie, Y.; He, Y.; Irwin, P.L.; Jin, T.; Shi, X. Antibacterial activity and mechanism of action of zinc oxide nanoparticles against *Campylobacter jejuni*. *Appl. Environ. Microb.* **2011**, *77*, 2325–2331. [[CrossRef](#)] [[PubMed](#)]
91. Reddy, L.S.; Nisha, M.M.; Joice, M.; Shilpa, P. Antimicrobial activity of zinc oxide (ZnO) nanoparticle against *Klebsiella pneumoniae*. *Pharm. Biol.* **2014**, *52*, 1388–1397. [[CrossRef](#)]
92. d'Água, R.B.; Branquinho, R.; Duarte, M.P.; Maurício, E.; Fernando, A.L.; Martins, R.; Fortunato, E. Efficient coverage of ZnO nanoparticles on cotton fibres for antibacterial finishing using a rapid and low cost in situ synthesis. *New J. Chem.* **2018**, *42*, 1052–1060.
93. Labrie, S.; Frois-Moniz, K.; Osburne, M.; Kelly, L.; Roggensack, S.; Sullivan, M.; Gearin, G.; Zeng, Q.; Fitzgerald, M.; Henn, M. Genomes of marine cyanopodoviruses reveal multiple origins of diversity. *Environ. Microbiol.* **2013**, *15*, 1356–1376. [[CrossRef](#)]
94. Sardella, D.; Gatt, R.; Valdramidis, V.P. Physiological effects and mode of action of ZnO nanoparticles against postharvest fungal contaminants. *Food Res. Int.* **2017**, *101*, 274–279. [[CrossRef](#)]
95. Rasha, E.; Monerah, A.; Manal, A.; Rehab, A.; Mohammed, D.; Doaa, E. Biosynthesis of Zinc Oxide Nanoparticles from *Acacia nilotica* (L.) Extract to Overcome Carbapenem-Resistant *Klebsiella Pneumoniae*. *Molecules* **2021**, *26*, 1919. [[CrossRef](#)]
96. Eskandari, M.; Haghghi, N.; Ahmadi, V.; Haghghi, F.; Mohammadi, S.R. Growth and investigation of antifungal properties of ZnO nanorod arrays on the glass. *Phys. B Condens. Matter* **2011**, *406*, 112–114. [[CrossRef](#)]